

Symmetry Abstractions for Hybrid Systems and their Applications

Hussein Sibai and Sayan Mitra
University of Illinois, Urbana IL 61801, USA
{sibai2,mitras}@illinois.edu

Abstract

A symmetry of a dynamical system is a map that transforms one trajectory to another trajectory. We introduce a new type of abstraction for hybrid automata based on symmetries. The abstraction combines different modes in a concrete automaton \mathcal{A} , whose trajectories are related by symmetries, into a single mode in the abstract automaton \mathcal{B} . The abstraction sets the guard and reset of an abstract edge to be the union of the symmetry-transformed guards and resets of the concrete edges. We establish the soundness of the abstraction using a forward simulation relation (FSR) and present several examples. Our abstraction results in simpler automata, that are more amenable for formal analysis and design. We illustrate an application of this abstraction in making reachability analysis faster and enabling unbounded time safety verification. We show how a fixed point of the reachable set computation of \mathcal{B} can be used to answer reachability queries for \mathcal{A} , even if the latter visits an infinite and unbounded sequences of modes. We present our implementation of the abstraction construction, the fixed point check, and the map that transforms abstract reachable sets to concrete ones in a software tool. Finally, we show the advantage of our method over existing ones, and the different aspects of our abstraction, in a sequence of experiments including scenarios with linear and nonlinear agents following waypoints.

Index Terms

hybrid systems, abstractions, symmetry, formal methods, reachability analysis.

I. INTRODUCTION

Hybrid system models bring together continuous and discrete behaviors [1]–[3], and have proven to be useful in the design and analysis of a wide variety of systems, ranging from automotive, medical, to manufacturing and robotics. Exact algorithmic solutions for many of the synthesis and analysis problems for hybrid systems are known to be computationally intractable [4]. Therefore, one aims to develop approximate solutions, and the main approach is to work with an *abstraction* of the hybrid system model. Roughly, an abstraction of a hybrid automaton \mathcal{A} is a simpler automaton \mathcal{B} that subsumes all behaviors of \mathcal{A} . For example, \mathcal{B} may have fewer variables than \mathcal{A} , or fewer modes, or it may have linear or rectangular dynamics approximating \mathcal{A} 's nonlinear dynamics. \mathcal{A} is called the *concrete*, and \mathcal{B} the *abstract* or *virtual* automaton. Ideally, \mathcal{B} is simpler and yet a useful over-approximation of \mathcal{A} , and the formal analysis and synthesis of \mathcal{B} is tractable.

Several important verification and synthesis techniques for hybrid systems have relied on abstractions. The early decidability results for verification of rectangular hybrid systems were based on creating discrete and finite state abstractions [4]–[6]. Decidability results based on abstractions for more general classes were presented in [7], [8]. In a sequence of papers [9]–[11], metric-based abstractions were developed for more general hybrid models and shown to be useful for both verification and synthesis. Techniques have been developed for automatically making abstractions more precise based on data and counterexamples [12]–[15]. Finally, several practical approaches have been proposed for computing abstractions based on linearization [16], state space partitioning [13], [17], and hybridization [18].

An important characteristic of dynamical systems that has *not* been explored for constructing abstractions in the literature is *symmetry*. Symmetry in a dynamical system $\dot{x} = f(x, p)$, with parameter p , is a map γ that transforms solutions (or *trajectories*) of the system to other trajectories. For example, consider a trajectory $\xi_0 = \xi(x_0, p, \cdot)$ of a vehicle, starting from x_0 and following waypoint p . When ξ_0 is *shifted* by a , the result $\gamma_a(\xi_0)$ is just the trajectory of the vehicle starting from $\gamma_a(x_0)$ following p' , $\xi'_0 = \xi(\gamma_a(x_0), p', \cdot)$. Here p' is p shifted by a . That is, the symmetry γ_a relates different trajectories of the system. This property has been used for studying stability of feedback systems [19], designing observers [20] and controllers [21], analyzing neural networks [22], and deriving conservation laws [23] using Noether's theorem [24].

Since both of ξ_0 and ξ'_0 are solutions of the system, and γ_a can compute ξ'_0 from ξ_0 , then, in a sense, f has some redundancy. A simpler version of f , would only have ξ_0 as a solution, and allows us to derive ξ'_0 using γ_a . In this paper, we create such simpler versions by defining symmetry-based abstractions for hybrid automata.

Given a hybrid automaton \mathcal{A} having a set of discrete states (or *modes*) P and a family of symmetry maps Φ , our abstraction partitions P to create the abstract automaton \mathcal{A}_v . Each *equivalent class* of the partition is represented by a single mode in \mathcal{A}_v . Any trajectory ξ of any mode $p \in P$, can be transformed using Φ to get a trajectory ξ_v of the representative abstract mode p_v , and vice versa. Accordingly, all concrete edges between any two equivalent mode classes would be represented with a single abstract edge. A set of concrete edges represented with the same abstract edge forms an equivalent edge class. The edges of \mathcal{A} are annotated with *guards* and *resets*. These dictate when the discrete transitions over the edges can be taken and how the state would be updated, respectively. The abstraction transforms the guards and resets of all concrete edges using Φ . Then, it unions all of the transformed guards and resets of an edge equivalent class to get the guard and reset of the corresponding abstract edge. This means that an execution of \mathcal{A}_v would transition over an edge e_v if any of the transformed guards of the edges of \mathcal{A} that e_v represents is satisfied. Moreover, the execution would split into several executions after a reset. Each of these executions start from a transformed version of the state defined by the reset of an edge of \mathcal{A} that is represented by e_v . We establish the soundness of this abstraction using a FSR (Theorem 3).

With several examples related to vehicles, we show that symmetry abstractions are natural. The abstraction can be useful for solving several problems related to tractability of synthesis and verification. In this paper, we focus on a particular application that is *reachability analysis*. Our abstraction accelerates reachability analysis and enables unbounded time safety verification because \mathcal{A}_v has fewer modes than \mathcal{A} . For safety verification, the reachset of \mathcal{A} ($\text{Reach}_{\mathcal{A}}$) rather than that of \mathcal{A}_v is what matters. We show that $\text{Reach}_{\mathcal{A}}$ can be retrieved from $\text{Reach}_{\mathcal{A}_v}$ using Φ (Section VI-C). In fact, we show in our experiments in Section VII, that computing $\text{Reach}_{\mathcal{A}_v}$ and then transforming it with Φ , is computationally less expensive than computing $\text{Reach}_{\mathcal{A}}$ directly. Since $\text{Reach}_{\mathcal{A}_v}$ is expected to be smaller than $\text{Reach}_{\mathcal{A}}$, its computation would reach a fixed point earlier than that of $\text{Reach}_{\mathcal{A}}$. Moreover, $\text{Reach}_{\mathcal{A}_v}$ might be a bounded set when $\text{Reach}_{\mathcal{A}}$ is not. This property enables unbounded safety verification. Using our method, the safety verification problem of \mathcal{A} changes from computing $\text{Reach}_{\mathcal{A}}$ and checking if it intersects with an unsafe set U , to checking if there exists a map in Φ that transforms $\text{Reach}_{\mathcal{A}_v}$ to intersect U (see Algorithm 1). The search over Φ for a map that transforms a bounded reachset $\text{Reach}_{\mathcal{A}_v}$ to intersect U would be easier than computing an unbounded reachset of a nonlinear automaton $\text{Reach}_{\mathcal{A}}$, where the latter might not even be feasible.

A. Summary of contributions

- We introduce a new type of abstraction for hybrid systems based on symmetries (Definition 5) and explain its construction with examples (Examples 1,2,3,4,5,6).
- We show that it is an abstraction using a FSR, and therefore, enjoys all the properties of standard abstractions (Theorem 3).
- We show the practical advantage of this abstraction in accelerating bounded verification. We also show that it enables unbounded-time safety verification of \mathcal{A} , using a data-structure called *Dictionary*, that stores the per-mode reachsets of \mathcal{A}_v (Algorithm 1 and Theorem 8).

- We present an implementation of our abstraction construction, a fixed-point check on the reachset computation, and the construction of *Dictionary*.
- We evaluate our implementation with experiments on a sequence of waypoint-following examples with scenarios having linear and nonlinear continuous dynamics, following different paths, using translation only or the combination of translation and rotation symmetries.

B. Reachability and symmetry: brief literature review

Reachability analysis is an essential tool in formal verification of hybrid systems. Significant strides have been made in reachability analysis of continuous time dynamical and hybrid systems in the past decade. Linear dynamical models with thousands, and even millions, of dimensions have been verified [25]–[27]. Nonlinear models of realistic systems ranging from engine control systems [28]–[31] to biomedical processes have been analyzed [32]–[34]. Software tools to solve the reachability problem have been developed [26], [35], [35]–[40]. These developments rely on advances in data-structures and dynamical systems theory results that exploit characteristics like sparsity and stability. Exploiting symmetries using the abstraction presented here will add a new methodology to this toolbox.

Symmetry was used to accelerate the safety verification of dynamical systems achieving promising results, in some cases by orders of magnitude speedups [41]–[43]. In [43], Maidens et al. used the Cartan moving frame method for symmetric nonlinear discrete-time dynamical systems to move from absolute representation of states to relative ones. That resulted in orders of magnitude speed up on the backward reachable set computation problem for checking if two Dubin vehicles would collide. In our paper, we consider hybrid systems, with discrete and continuous dynamics, and reduce the number of modes of the automaton, instead of considering pure-discrete dynamics and reducing the dimension of the state space as in [43].

In [41], we utilized symmetry of an autonomous dynamical system to cache and retrieve its reachsets using symmetry transformations. When given a continuous family of symmetry transformations, we were able to reduce the dimensionality of the reachsets that had to be computed, achieving orders of magnitude speedup in verification time. In contrast, this paper, we focus on hybrid systems instead of continuous dynamical systems. In [42], we extended the result of [41] to the parameterized dynamical systems and multi-agent settings. That allowed us to tackle hybrid automata as well. We viewed the different modes of an automaton as parameterized dynamical systems. We constructed a representative mode p^* of all the modes, using symmetry, and then used p^* as a proxy to share reachsets across different modes using a cache. However, in [42], we did not develop the general abstraction-based view of symmetry (Definition 5 and Theorem 3). As a result, we did not have a fixed point analysis (Theorem 6 and Corollary 7), and we were not able to verify unbounded-time safety properties.

II. MODEL AND PROBLEM STATEMENT

Notations: We denote by \mathbb{N} , \mathbb{R} , and $\mathbb{R}^{\geq 0}$ the sets of natural numbers, real numbers and non-negative reals, respectively. Given a finite set S , its cardinality is denoted by $|S|$. The length of a finite sequence seq is denoted by $seq.len$ and its elements between i and j , inclusive, by $seq[i : j]$. Given $N \in \mathbb{N}$, we denote by $[N]$ the set $\{0, \dots, N - 1\}$. Given two vectors $v \in \mathbb{R}^n$ and $u \in \mathbb{R}^m$, we define $[v, u]$ to be the vector of length $n + m$ that results from appending u to v . Given $\varepsilon \in (\mathbb{R}^{\geq 0})^n$, we denote by $B(v, \varepsilon)$ the n -dimensional hyper-rectangle centered at v with i^{th} dimension sides having length $\varepsilon[i]$, for all $i \in [n]$. Given a hyper-rectangle $H \subseteq \mathbb{R}^n$ and a set of indices $L \subseteq [n]$, we denote the restriction of H to the indices in L by $H[L]$. We denote $diag(v)$ to be the diagonal matrix with diagonal v . Given a function $\gamma: \mathbb{R}^n \rightarrow \mathbb{R}^n$ and a set $S \subseteq \mathbb{R}^n$, as usual, we lift the function to subsets of \mathbb{R}^n , and define $\gamma(S) = \{\gamma(x) \mid x \in S\}$. We also lift it to vectors of \mathbb{R}^n and define $\gamma(v) = [\gamma(v_1), \gamma(v_2), \dots, \gamma(v_k)]$, for any $v \in \mathbb{R}^{n \times k}$. We define $\arctan_2(y, x)$ to be the phase of the complex number $x + jy$.

A. Hybrid dynamics

In this paper, we will use a standard hybrid automaton modeling framework for defining cyber-physical systems [44]–[46].

Definition 1: A *hybrid automaton* is a tuple $\mathcal{A} = \langle X, P, X_{init}, p_{init}, E, guard, reset, f \rangle$, where

- (a) $X \subseteq \mathbb{R}^n$ is the continuous state space and P is a (possibly infinite) set of discrete states. Continuous states are simply called *states* and the discrete ones are called *modes* or *parameters*.
- (b) $X_{init} \subseteq X$ is a set of possible initial states and $p_{init} \in P$ is the initial mode,
- (c) $E \subseteq P \times P$ is the set of directed edges over modes that define mode transitions,
- (d) $guard : E \rightarrow 2^X$ gives the set of states from which an edge transition is enabled,
- (e) $reset : X \times E \rightarrow 2^X$ gives the updated (post) state after a transition is taken, and
- (f) $f : X \times P \rightarrow X$ is a *dynamic function* that defines the continuous evolution. It is Lipschitz continuous in the first argument.

The dynamic function $f(\cdot, p)$ define the continuous state evolution in each mode $p \in P$. A function $\xi : X \times P \times \mathbb{R}^{\geq 0} \rightarrow X$ is a *trajectory* of \mathcal{A} if ξ is differentiable in its third argument, and given an initial state $x_0 \in X$ and a mode $p \in P$, $\xi(x_0, p, 0) = x_0$ and for all $t \in \mathbb{R}^{\geq 0}$,

$$\frac{d}{dt} \xi(x_0, p, t) = f(\xi(x_0, p, t), p). \quad (1)$$

The trajectory ξ is the unique solution of (1) starting from x_0 , since f is Lipschitz continuous. We say that $\xi(x_0, p, t)$ is the state of (1) at time t starting from x_0 in mode p . When x_0 and p are clear from context, we denote $\xi(x_0, p, t)$ by $\xi(t)$, for simplicity. For any time-bounded trajectory ξ , i.e. defined over a finite interval in the third argument, $dur(\xi)$ is its last time point. The first and last state in such a trajectory are denoted by $\xi.fstate$ and $\xi.lstate$, respectively.

The edge set E , the *guard*, and the *reset* together define the discrete transitions. For simplicity, for an edge $e = (p, p') \in E$, we denote its source mode p by $e.src$ and its destination mode p' by $e.dest$. A sequence of modes p_0, p_1, \dots , where for all $i \geq 0$, $(p_i, p_{i+1}) \in E$ is called a *path*. Moreover, we abuse notation and denote $guard((p, p'))$ by $guard(p, p')$. Then, $guard(p, p')$ is the set from which a transition from mode p to mode p' is possible. From a state $x \in guard(p, p')$, the post-state x' after the transition has to be in $reset(x, (p, p'))$. Such state-mode pairs $((x, p), (x', p'))$ define the transitions of \mathcal{A} and we write $(x, p) \rightarrow (x', p')$. Note that there are no urgent transitions here, and guards may be ignored.

The semantics of a hybrid automaton is defined by executions which are sequences of trajectories and transitions. An *execution* of \mathcal{A} is a sequence of pairs of trajectories and modes $\sigma = (\xi_0, p_0), (\xi_1, p_1), \dots$, where (a) each ξ_i is a trajectory of \mathcal{A} , (b) each $(\xi_i.lstate, p_i) \rightarrow (\xi_{i+1}.fstate, p_{i+1})$ is a transition as defined above. A *finite* and *time-bounded* execution has a finite number of discrete transitions and all of its trajectories are time-bounded. The duration of a finite and time-bounded execution $\sigma = (\xi_0, p_0), (\xi_1, p_1) \dots (\xi_k, p_k)$ is $dur(\sigma) = \sum_i dur(\xi_i)$ and its last state is $\sigma.lstate = \xi_k.lstate$.

Finally, fix $J \in \mathbb{N}$; $Exec_{\mathcal{A}}(J)$ is the set of all executions of \mathcal{A} with at most J transitions; When the transitions are unbounded, it is denoted by $Exec_{\mathcal{A}}$. We define the set of *reachable states* as:

$$Reach_{\mathcal{A}} = \{x \in X \mid \exists \sigma \in Exec_{\mathcal{A}}, \sigma.lstate = x\}. \quad (2)$$

$Reach_{\mathcal{A}}(J)$ is the reachset restricted to executions with at most J transitions.

Example 1 (Robot following waypoints) Consider a robot following a sequence of waypoints $\{w_i \in \mathbb{R}^2 \mid i \in [4]\}$ on the plane connected with directed roads $\{r_i \in \mathbb{R}^4 \mid i \in [5]\}$ forming an axis-aligned rectangle centered at the origin (see Figure 1a). The robot starts from an arbitrary point in some initial set $X_{init} \subset \mathbb{R}^3$. We fix rectangles with dimensions $\varepsilon_0 \in (\mathbb{R}^{\geq 0})^2$ or $\varepsilon_1 \in (\mathbb{R}^{\geq 0})^2$. We say that it reached the first waypoint w_0 following road r_0 if it is located in the rectangle $B(w_0, \varepsilon_0)$. If it was following road r_1 instead, we say it reached w_0 if it is located in the smaller rectangle $B(w_0, \varepsilon_1)$. Moreover, for any $i \in \{1, 2, 3\}$, we say that it reached the waypoint w_i following road r_i if it is located in the rectangle $B(w_i, \varepsilon_1)$.

To formalize the dynamics of the robot in this scenario, we construct a corresponding hybrid automaton. We use the four waypoints as four modes of the automaton, i.e. $P = \{w_1, w_2, w_3, w_4\}$. Consequently,

whether starting from X_{init} or coming from w_3 , i.e. following road r_0 or road r_4 , the robot would be in the same mode which corresponds to following w_0 . Thus, one should not confuse the roads of the path in Figure 1a with the edges of the automaton that we will construct. Now, we fix $\varepsilon_0 = [1, 1.4]$ and $\varepsilon_1 = [0.6, 1]$. The resulting hybrid automaton is shown in Figure 1b and would be formally defined as: $W = \langle X, P, X_{init}, p_{init}, E, guard, reset, f \rangle$:

- (a) $X \subseteq \mathbb{R}^3$, representing the position and orientation with respect to the $x[0]$ -axis, and $P = \{p_i = w_i \mid i \in [4]\}$,
- (b) $X_{init} = B([-4.5, -0.5, -\frac{\pi}{4}], [0.8, 0.8, \frac{\pi}{2}])$, $p_{init} = p_0 = w_0$,
- (c) $E = \{e_0 = (p_0, p_1), e_1 = (p_1, p_2), e_2 = (p_2, p_3), e_3 = (p_3, p_0)\}$,
- (d)

$$guard(e_i) = \begin{cases} (B(w_i, \varepsilon_0) \cup B(w_i, \varepsilon_1)) \times \mathbb{R}, & \text{if } i = 0, \\ B(w_i, \varepsilon_1) \times \mathbb{R}, & \text{if } i = \{1, 2, 3\}, \end{cases}$$

- (e) $\forall x \in X, e \in E$,

$$reset(x, e) = \{x\}, \quad (3)$$

is the identity map, and

- (f) $\forall x \in X, \forall p \in P$,

$$f(x, p) = \frac{dx}{dt} = \begin{bmatrix} v \cos(x[2]) \\ v \sin(x[2]) \\ 2v \sin(\alpha)/L \end{bmatrix}, \text{ where} \quad (4)$$

$\alpha = \arctan_2(p[1] - x[1], p[0] - x[0]) - x[2]$ and v and L are the fixed speed and length of the robot [47].

III. SYMMETRY AND EQUIVARIANT DYNAMICAL SYSTEMS

In this section, we present an existing definition of symmetry for dynamical systems with parameters and a sufficient condition for a map to be a symmetry.

A symmetry map γ acts on the state space X , i.e. $\gamma: X \rightarrow X$, such that given a solution of the system, it maps it to another valid solution.

Definition 2 (Definition 2 in [48]) Let Γ be a group of maps acting on X . We say that $\gamma \in \Gamma$ is a symmetry of (1) if it is differentiable, invertible, and for any solution $\xi(x_0, p, \cdot)$, $\gamma(\xi(x_0, p, \cdot))$ is a solution as well.

Fortunately, a map can be checked if it is a symmetry of a system by analyzing whether it commutes with its dynamic function.

Definition 3 ([48]) The dynamic function $f: X \times P \rightarrow X$ is said to be Γ -equivariant if for any $\gamma \in \Gamma$, there exists $\rho: P \rightarrow P$ such that,

$$\forall x \in X, \forall p \in P, \frac{\partial \gamma}{\partial x} f(x, p) = f(\gamma(x), \rho(p)). \quad (5)$$

The following theorem shows that it is enough to check the condition in equation (5) to prove that a map is a symmetry.

Theorem 1 (part of Theorem 10 of [48]) If f is Γ -equivariant, then all maps in Γ are symmetries of (1). Moreover, for any $\gamma \in \Gamma$, map $\rho: P \rightarrow P$ that satisfies equation (5), $x_0 \in X$, and $p \in P$, $\gamma(\xi(x_0, p, \cdot)) = \xi(\gamma(x_0), \rho(p), \cdot)$.

Note that if γ in Theorem 1 is a linear function of the state, i.e. $\gamma(x) = Ax$, for some $A \in \mathbb{R}^{n \times n}$, the condition in equation (5) for equivariance becomes $\gamma(f(x, p)) = f(\gamma(x), \rho(p))$.

Example 2 (Robot origin translation symmetry) Consider the robot presented in Example 1, and maps γ_{ot} and ρ_{ot} that translate the origin of the plane to a new origin $p^* \in \mathbb{R}^2$. Let $\gamma_{ot}: \mathbb{R}^3 \rightarrow \mathbb{R}^3$ and $\rho_{ot}: \mathbb{R}^2 \rightarrow \mathbb{R}^2$

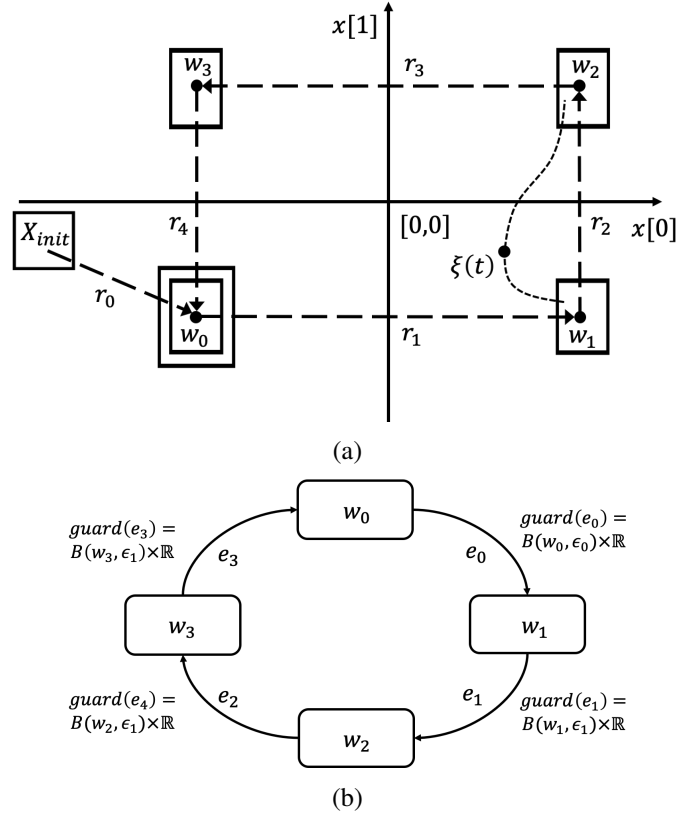


Fig. 1: (1a) A robot, with a state containing its position and orientation, following a sequence of 2D waypoints forming a rectangle starting from its initial set X_{init} . It reaches a waypoint if it reaches the rectangle centered at it. It has to reach the larger rectangle centered at w_0 when starting from X_{init} . (1b) The state machine representing the discrete transitions of the hybrid automaton W describing the scenario in (1a). The resets are omitted since they are the identity map for all the edges.

be defined as:

$$\gamma_{ot}(x) = [x[0 : 1] - p^*, x[2]], \quad (6)$$

$$\rho_{ot}(p) = (p - p^*), \quad (7)$$

Then, $\frac{\partial \gamma_{ot}}{\partial x} f(x, p) = \frac{\partial \gamma_{ot}}{\partial x} \frac{dx}{dt} = I_3 \times f(x, p) = f(x, p)$, where α is as in equation (4) and I_3 is the 3×3 identity matrix. Moreover,

$$f(\gamma_{ot}(x), \rho_{ot}(p)) = \begin{bmatrix} v \cos(x[2]) \\ v \sin(x[2]) \\ 2v \sin(\alpha')/L \end{bmatrix}, \text{ where} \quad (8)$$

$\alpha' = \arctan_2(p[1] - p^*[1] - (x[1] - p^*[1]), p[0] - p^*[0] - (x[0] - p^*[0])) - x[2] = \alpha$. Then, for all $x \in X$ and $p \in P$, $\frac{\partial \gamma}{\partial x} f(x, p) = f(\gamma_{ot}(x), \rho_{ot}(p))$, and γ_{ot} is a symmetry of f . Figure 2 shows the new state $\xi(t) - p^*$ and new parameter $w_2 - p^*$ representing mode p_2 of the robot of Figure 1a after translating the origin to p^* using γ_{ot} and ρ_{ot} of this example.

IV. VIRTUAL OR ABSTRACT HYBRID AUTOMATON

In this section, we present our symmetry-based abstraction of hybrid automata along with the corresponding FSR. Our abstract automata have fewer numbers of modes and edges, than their concrete counterparts.

Our abstraction is an extension of the concept of virtual system for parameterized dynamical systems that we defined in [42], to hybrid systems. Throughout the paper, we use subscript v to denote the variables and functions of the abstract (or virtual) automaton and no subscript for those of the concrete one.

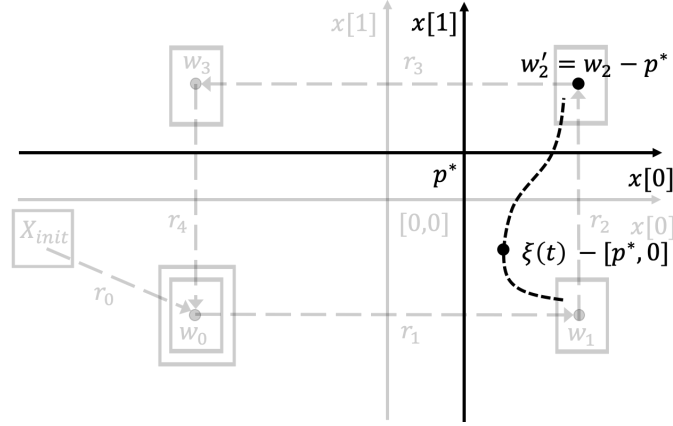


Fig. 2: Changing the origin of the coordinate system to p^* in Figure 1a, does not affect the intrinsic behavior of the robot, but only translates the states in its trajectories. Such a translation is a valid symmetry of the robot dynamics.

A. Creating the virtual model

In order to create the virtual model, a family of symmetries is needed. This is formalized below.

Definition 4 (virtual map) Given a hybrid automaton \mathcal{A} , a *virtual map* is a set

$$\Phi = \{(\gamma_p, \rho_p)\}_{p \in P}, \quad (9)$$

where for every $p \in P$, $\gamma_p : X \rightarrow X$, $\rho_p : \mathbb{R}^m \rightarrow \mathbb{R}^m$, and they satisfy equation (5).

Given \mathcal{A} and a virtual map Φ , each γ_p is called a *virtual state map* and each ρ_p is called a *virtual mode map*. From Theorem 1, it follows that these maps transform trajectories in mode p to trajectories in mode $\rho_p(p)$. Using a virtual map Φ of \mathcal{A} , we can define the function $rv : \mathbb{R}^m \rightarrow \mathbb{R}^m$, where for all $p \in P$:

$$rv(p) = \rho_p(p). \quad (10)$$

This function will be used in Definition 5 to map concrete modes to virtual ones. Moreover, its inverse will be used to map virtual modes to the sets of concrete modes, or the equivalent mode classes, that they represent.

Definition 5 (virtual model) Given a hybrid automaton \mathcal{A} , and a virtual map Φ , the resulting *abstract (virtual) hybrid automaton* is:

$$\mathcal{A}_v = \langle X_v, P_v, X_{init,v}, p_{init,v}, E_v, guard_v, reset_v, f_v \rangle, \text{ where}$$

- (a) $X_v = X$ and $P_v = rv(P)$
- (b) $X_{init,v} = \gamma_{p_{init}}(X_{init})$ and $p_{init,v} = rv(p_{init})$,
- (c) $E_v = rv(E) = \{(rv(p_1), rv(p_2)) \mid e = (p_1, p_2) \in E\}$
- (d) $\forall e_v \in E_v$,

$$guard_v(e_v) = \bigcup_{e \in rv^{-1}(e_v)} \gamma_{e.src}(guard(e)),$$

- (e) $\forall x_v \in X_v, e_v \in E_v$,

$$reset_v(x_v, e_v) = \bigcup_{e \in rv^{-1}(e_v)} \gamma_{e.dest}(reset(\gamma_{e.src}^{-1}(x_v), e)), \text{ and}$$

- (f) $\forall p_v \in P_v, \forall x \in X, f_v(x, p_v) = f(x, p_v)$.

The trajectories and executions of the virtual hybrid automaton \mathcal{A}_v are defined in the same way as in Definition 1.

Example 3 (Robot virtual system) Consider the scenario described in Figure 1a and its corresponding hybrid automaton W defined in Example 1. To construct its virtual automaton, we need a virtual map Φ

first. For every $p \in P$, we define γ_p and ρ_p to be the origin translation maps γ_{ot} and ρ_{ot} that we presented in Example 2. Recall that in that example, we needed to define p^* that we want to translate the origin to. For this example, for each $p \in P$, we choose p^* to be equal to p . Figure 3a shows a visualization of γ_{p_2} and ρ_{p_2} . In that figure, the waypoint w_2 , which is the concrete mode p_2 , becomes the origin p_v after applying ρ_{p_2} . Hence, p_2 gets represented in the virtual automaton by the virtual mode p_v , as shown in Figures 3b and 3c.

The set $guard(e_2)$ of \mathcal{A} , becomes $B(p_v, \varepsilon_1) \times \mathbb{R}$, after applying γ_{p_2} . This rectangle will be part of the guard of the virtual mode p_v , as specified in Definition 5 part (d). Its projection to the first two dimensions is shown as the rectangle $B(p_v, \varepsilon_0)$ centered at the origin p_v in Figure 3b.

Figure 3a also shows that the rectangle $B(w_1, \varepsilon_1)$, which is $guard(e_1)[0 : 1]$, becomes $B(w_1 - w_2, \varepsilon_0)$ a rectangle centered at $w_1 - w_2$, after applying γ_{p_2} . Recall that the reset of any edge of W is just the identity map. Hence, the rectangle centered at $w_1 - w_2$ represents $\gamma_{p_2}(reset(guard(e_1)), e_1)[0 : 1]$. This will be part of the set of possible reset states per part (e) of Definition 5. It is shown as the rectangle in the negative side of the $x[1]$ -axis in Figure 3b.

The illustration above for p_2 would be repeated for every $p \in P$, to construct the virtual system shown in Figure 3b.

In summary, the resulting virtual automaton would be: $W_v = \langle X_v, P_v, X_{init,v}, p_{init,v}, E_v, guard_v, reset_v, f_v \rangle$, where

- (a) $X_v = X = \mathbb{R}^3$ and $P_v = \{p_v = [0, 0]\}$,
- (b) $X_{init,v}$ is $\gamma_{p_{init}}(X_{init})$ which is the translation of the center of X_{init} from $[-4.5, 0.5, -\frac{\pi}{4}]$ to $[-2, 1, -\frac{\pi}{4}]$, $p_{init,v}$ is the only mode p_v , which is the origin,
- (c) $E_v = \{e_v = [p_v, p_v]\}$, since all modes are mapped to p_v , all the edges map to the same virtual edge e_v ,
- (d)

$$guard_v(e_v) = B(p_v, \varepsilon_0) \times \mathbb{R}. \quad (11)$$

It is the union of all guards of all the edges mapped to rectangles centered at the origin. The guards of e_1, e_2 , and e_3 would be mapped to $B(p_v, \varepsilon_1) \times \mathbb{R}$, while that of e_0 would be mapped to $B(p_v, \varepsilon_0) \times \mathbb{R}$,

- (e) $\forall x_v \in X_v$,

$$reset_v(x_v, e_v) = \{\gamma_{p_1}(\gamma_{p_0}^{-1}(x_v)), \gamma_{p_2}(\gamma_{p_1}^{-1}(x_v)), \gamma_{p_3}(\gamma_{p_2}^{-1}(x_v)), \gamma_{p_0}(\gamma_{p_3}^{-1}(x_v))\}, \text{ and}$$

- (f) $\forall x_v \in X_v, f_v(x, p_v) = f(x, p_v)$, it is the dynamics of equation (4) in Example (1) going to the origin. The reset of the guard is the set of all possible reseted states. It is shown as the rectangles along the axes in Figure 3b.

B. Forward simulation relation (FSR): from concrete to virtual

In this section, we establish a correspondence from the executions of the concrete system to those of the virtual one through a FSR [45], [46], [49]. A FSR is a standard approach to describe the similarity of behavior of two different hybrid automata.

Definition 6 (FSR [45]) A *forward simulation relation* from hybrid automaton \mathcal{A}_1 to another one \mathcal{A}_2 , is a relation $\mathcal{R} \subseteq (X_1 \times P_1) \times (X_2 \times P_2)$, such that

- (a) for any initial $x_{0,1} \in X_{init,1}$, there exists a state $x_{0,2} \in X_{init,2}$, such that $(x_{0,1}, p_{init,1}) \mathcal{R} (x_{0,2}, p_{init,2})$,
- (b) For any discrete transition $(x_1, p_1) \rightarrow (x'_1, p'_1)$ of \mathcal{A}_1 and $(x_2, p_2) \in X_2 \times P_2$, where $(x_1, p_1) \mathcal{R} (x_2, p_2)$, there exists $(x'_2, p'_2) \in X_2 \times P_2$ such that $(x_2, p_2) \rightarrow (x'_2, p'_2)$ is a discrete transition of \mathcal{A}_2 and $(x'_1, p'_1) \mathcal{R} (x'_2, p'_2)$, and
- (c) For any solution $\xi_1(x_1, p_1, \cdot)$ of \mathcal{A}_1 and pair $(x_2, p_2) \in X_2 \times P_2$, such that $(x_1, p_1) \mathcal{R} (x_2, p_2)$, there exists a solution $\xi_2(x_2, p_2, \cdot)$, where $dur(\xi_1) = dur(\xi_2)$ and $(\xi_1.lstate, p_1) \mathcal{R} (\xi_2.lstate, p_2)$.

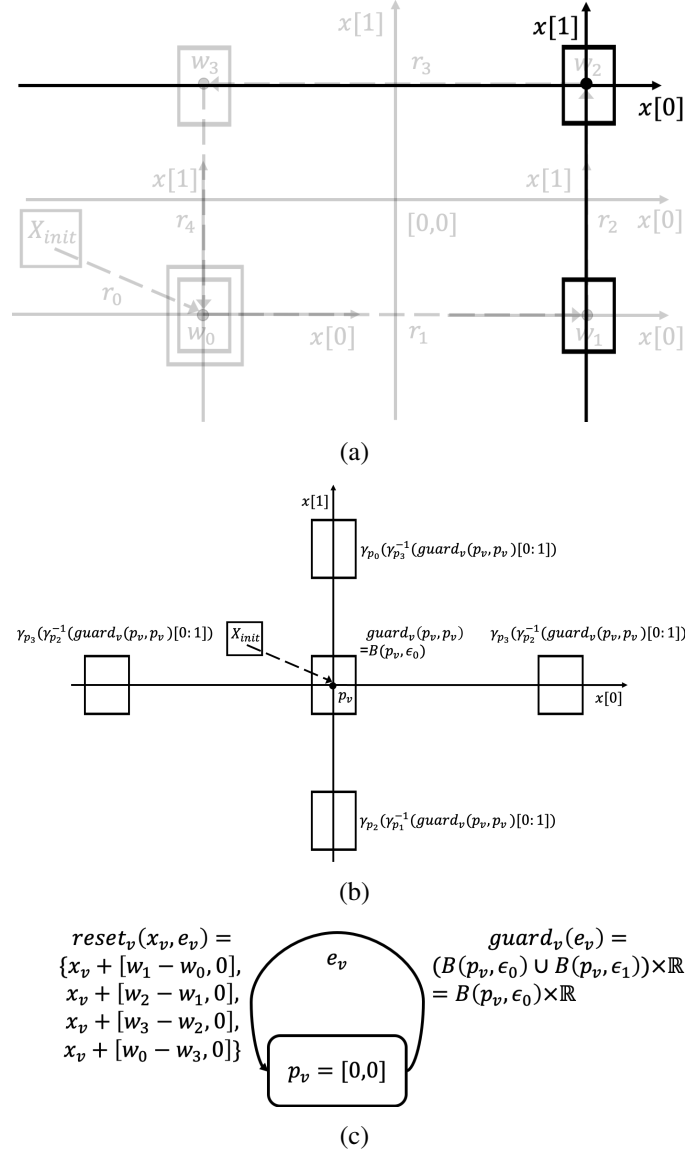


Fig. 3: (3a) the symmetry transformation that changes the origin of the plane of Figure 1a to the waypoint w_2 . (3b) shows the virtual initial sets, guards and reset guards of the virtual automaton of Figure 1a after choosing the virtual map to be the set of origin translations to the waypoints. (3c) shows the resulting hybrid automaton \mathcal{A}_v .

Existence of a FSR implies that for any execution of \mathcal{A}_1 there is a corresponding related execution of \mathcal{A}_2 . The following theorem is an adoption of Corollary 4.23 of [45] into our hybrid modeling framework.

Theorem 2 (executions correspondence [45]) If there exists a forward simulation relation \mathcal{R} from \mathcal{A}_1 to \mathcal{A}_2 , then for every execution σ_1 of \mathcal{A}_1 , there exists a corresponding execution σ_2 of \mathcal{A}_2 such that

- (a) $\sigma_1.\text{len} = \sigma_2.\text{len}$,
- (b) $\forall i \in [\sigma_1.\text{len}], \text{dur}(\xi_{1,i}) = \text{dur}(\xi_{2,i})$, and
- (c) $\forall i \in [\sigma_1.\text{len}], (\xi_{1,i}.\text{lstate}, p_{1,i}) \mathcal{R} (\xi_{2,i}.\text{lstate}, p_{2,i})$.

Now we introduce a FSR from the concrete hybrid automaton to the virtual one.

Theorem 3 (FSR: concrete to virtual) Consider the relation $\mathcal{R}_{rv} \subseteq (X \times P) \times (X_v \times P_v)$ defined as $(x, p) \mathcal{R}_{rv} (x_v, p_v)$ if and only if:

- (a) $x_v = \gamma_p(x)$, and
- (b) $p_v = rv(p)$.

Then, \mathcal{R}_{rv} is a forward simulation relation from \mathcal{A} to \mathcal{A}_v .

Proof: \mathcal{R}_{rv} satisfies Definition 6.(a) since: for any $x_0 \in X_{init}$, $\gamma_{p_{init}}(x_0) \in X_{init,v}$, and $p_{init,v} = rv(p_{init})$, by Definition 5.(b).

To prove that \mathcal{R}_{rv} satisfies Definition 6.(b), fix a discrete transition $(x, p) \rightarrow (x', p')$ of \mathcal{A} and $(x_v, p_v) \in X_v \times P_v$ such that $(x, p, x_v, p_v) \in \mathcal{R}_{rv}$. We will show that if we choose $x'_v = \gamma_{p'}(x_v)$ and $p'_v = rv(p')$, then $(x'_v, p'_v) \in X_v \times P_v$, $(x', p', x'_v, p'_v) \in \mathcal{R}_{rv}$, and $(x_v, p_v) \rightarrow (x'_v, p'_v)$ is a valid discrete transition of \mathcal{A}_v .

First, $x'_v \in X_v$ since $x' \in X$, $\gamma_{p'}$ is a map from X to X , and by Definition 5.(a), $X = X_v$. Moreover, $p'_v \in P_v$ by Definition 5.(a). Second, $(x', p', x'_v, p'_v) \in \mathcal{R}_{rv}$ since $x'_v = \gamma_{p'}(x')$ and $p'_v = rv(p')$. Third, fix $e = (p, p')$. Then, by the definition of discrete transitions of \mathcal{A} , $x \in guard(e)$ and $x' \in reset(x, e)$. Also, from the definition of E_v in Definition 5.(c), the edge $e_v = (p_v, p'_v) \in E_v$. Also, by the definition of \mathcal{R}_{rv} and the assumption that x and x_v are related under \mathcal{R}_{rv} , $x_v = \gamma_p(x)$. That means that $x_v \in \gamma_p(guard(e))$, since $x \in guard(e)$. But, by Definition 5.(d), $\gamma_p(guard(e)) \subseteq guard_v(e_v)$. Then, $x_v \in guard_v(e_v)$. Moreover, since $x' \in reset(x, e)$ and $x = \gamma_p^{-1}(x_v)$, then $x' \in reset(\gamma_p^{-1}(x_v), e)$. Hence, $x'_v = \gamma_{p'}(x') \in \gamma_{p'}(reset(\gamma_p^{-1}(x_v), e))$. Using Definition 5.(e), we know that $\gamma_{p'}(reset(\gamma_p^{-1}(x_v), e)) \subseteq reset_v(x_v, e_v)$. We have $x'_v \in reset_v(x_v, e_v)$. Therefore, $(x_v, p_v) \rightarrow (x'_v, p'_v)$ is a valid discrete transition of \mathcal{A}_v .

To prove that \mathcal{R}_{rv} satisfies Definition 6.(c), fix a solution $\xi(x, p, \cdot)$ of \mathcal{A} and a pair $(x_v, p_v) \in X_v \times P_v$, such that $(x, p, x_v, p_v) \in \mathcal{R}_{rv}$. Then, we will show that $dur(\xi) = dur(\xi_v)$ and $(\xi(x, p, dur(\xi)), p, \xi_v(x_v, p_v, dur(\xi)), p_v) \in \mathcal{R}_{rv}$. Since x and x_v are related under \mathcal{R}_{rv} , then $x_v = \gamma_p(x)$. Moreover, using Theorem 1, $\forall t \in dur(\xi)$, $\xi(\gamma_p(x), \rho_p(p), t) = \gamma_p(\xi(x, p, t))$. But, $rv(p) = p_v$ and using Definition 5.(f), $\xi(\gamma_p(x), \rho_p(p), \cdot) = \xi_v(\gamma_p(x), p_v, \cdot)$, which is a solution of \mathcal{A}_v starting from $\gamma_p(x) = x_v$. In addition, from the assumption that the guards are optional, we can choose ξ_v that does not transition before $dur(\xi)$. Therefore, $\forall t \in dur(\xi)$, $(\xi(x, p, t), p, \xi_v(x_v, p_v, t), p_v) \in \mathcal{R}_{rv}$. ■

Definition 7: Given a hybrid automaton \mathcal{A} and a virtual map Φ , we denote the corresponding virtual automaton by $\mathcal{A}_{v,\phi}$ and the resulting FSR of Theorem 3, by \mathcal{R}_ϕ .

The following corollary is also an adoption of Theorem 4.2 of [45] into our hybrid automaton framework.

Corollary 4 (Theorem 4.2 in [45]) Let A, B and C be three hybrid automata and Φ_{AB} and Φ_{BC} be two virtual maps such that $B = A_{v,\Phi_{AB}}$ and $C = B_{v,\Phi_{BC}}$ with corresponding FSRs \mathcal{R}_{AB} and \mathcal{R}_{BC} . Then, $C = A_{v,\Phi_{AC}}$ is the virtual automaton of A with FSR $\mathcal{R}_{AB} \circ \mathcal{R}_{BC}$ and virtual map $\Phi_{AC} = \Phi_{AB} \circ \Phi_{BC}$, where \circ is the composition operator.

Corollary 4 shows that we can apply symmetries in sequence to get hierarchical levels of abstractions of \mathcal{A} .

It is worth noting that there may not be a forward simulation relation from \mathcal{A}_v to \mathcal{A} . The guard and reset of an edge e_v of \mathcal{A}_v are the union of all the transformed versions of the guards and resets of the edges of \mathcal{A} that get mapped to e_v . Hence, some discrete transitions in \mathcal{A}_v may not have corresponding ones in \mathcal{A} . For example, consider two edges $e_1 = (p_{11}, p_{12})$ and $e_2 = (p_{21}, p_{22})$ of \mathcal{A} with $rv(e_1) = rv(e_2) = e_v = (p_{v1}, p_{v2})$, an edge of \mathcal{A}_v . Then, a transition over e_v would be allowed in \mathcal{A}_v with reseted state being $\gamma_{p_{22}}(reset(x_v, e_2))$ if $x_v \in \gamma_{p_{11}}(guard(e_1))$. Such a transition may not have a correspondent one in \mathcal{A} , since it resembles a transition from p_{11} to p_{22} . Thus, some executions of \mathcal{A}_v may not have corresponding executions in \mathcal{A} .

V. DIFFERENT VIRTUAL MAPS LEAD TO DIFFERENT ABSTRACTION

In this section, we show that the same scenario can result in different abstractions when different symmetries are applied. This multitude of modeling approaches would serve different purposes for the abstraction user.

We follow the same sequence of presentation as that of Examples 1, 2, and 3: first, we show a new hybrid automaton modeling of scenario in Figure 1a in Example 4, we then show a corresponding symmetry map in Example 5, and finally, construct a virtual map and the corresponding virtual automaton in Example 6.

Example 4 (Modeling the scenario in Figure 1a with roads as modes) Consider the same scenario described in Figure 1a. In this example, instead of defining the modes of the hybrid automaton to be the waypoints, suppose we define the modes to be the roads. In each mode, the robot would follow the destination waypoint of the corresponding road. We annotate the components of automaton W of

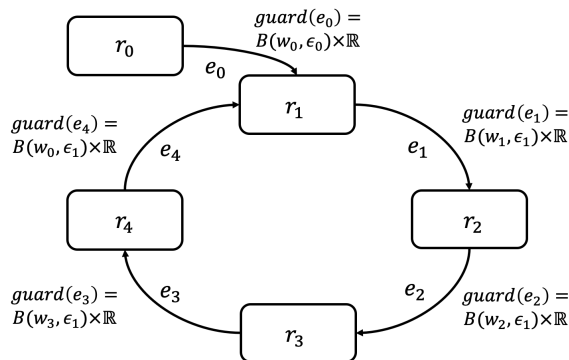


Fig. 4: The state machine representing the discrete transitions of the hybrid automaton R describing the scenario in Figure 1a with the roads being the modes. The resets are omitted since they are just the identity map for all the modes.

Example 1 with a subscript W and define the resulting automaton of this example as follows: $R = \langle X, P, X_{init}, p_{init}, E, guard, reset, f \rangle$ is shown in Figure 4, where

- (a) $X = X_W \subseteq \mathbb{R}^3$, same as that of Example 1, and $P = \{p_i = r_i \mid i \in [5]\}$, the set of roads in Figure 1a,
- (b) $X_{init} = X_{init,W}$ and $p_{init} = p_0$,
- (c) $E = \{e_0 = (p_0, p_1), e_1 = (p_1, p_2), e_2 = (p_2, p_3), e_3 = (p_3, p_4), e_4 = (p_4, p_1)\}$,
- (d)

$$guard(e_i) = \begin{cases} B(w_i, \epsilon_0) \times \mathbb{R}, & \text{if } i = 0, \\ B(w_i, \epsilon_1) \times \mathbb{R}, & \text{if } i = \{1, 2, 3, 4\}. \end{cases}$$

- (e) $\forall x \in X, e \in E,$

$$reset(x, e) = \{x\},$$

is the identity map, and

- (f) $\forall x \in X, \forall p \in P,$

$$f(x, p) = f_W(x, p.dest). \quad (12)$$

Example 5 (Robot coordinate transformation symmetry) We consider the new concrete model introduced in Example 4 of the scenario described in Figure 1a. Fix a vector $p^* \in \mathbb{R}^4$, where the first two coordinates $p^*.src$ define the start point and the last two coordinates $p^*.dest$ specifying the end point in the plane. Such a p^* is similar to the roads in Figure 1a. We define $\gamma_{ct} : X \rightarrow X$ and $\rho_{ct} : P \rightarrow P$ to be the maps that transform the coordinate system of the plane where the robot and roads reside. These maps transform it so that p^* will be collinear with the $x[0]$ -axis and $p^*.dest$ be the origin of the system. Formally, for every $x \in X$ and $p \in P$,

$$\gamma_{ct}(x) = [\mathbf{R}_\theta(x[0:1] - p^*.dest), x[2] - \theta], \quad (13)$$

$$\rho_{ct}(p) = [\mathbf{R}_\theta(p.src - p^*.dest), \mathbf{R}_\theta(p.dest - p^*.dest)], \quad (14)$$

where $\theta = \arctan_2(p^*.dest[1] - p^*.src[1], p^*.dest[0] - p^*.src[0])$ and

$$\mathbf{R}_\theta = \begin{bmatrix} \cos(\theta) & \sin(\theta) \\ -\sin(\theta) & \cos(\theta) \end{bmatrix} \quad (15)$$

is the rotation matrix with angle θ . Then, we can check with simple algebra, that for all $x \in X$ and $p \in P$, $\frac{\partial \gamma_{ct}}{\partial x} f(x, p) = f(\gamma_{ct}(x), \rho_{ct}(p))$.

Example 6 (Robot virtual system with a coordinate transformation virtual map) Consider the scenario described in Example 1 and Figure 1a and its hybrid automaton modeling in Example 4. To construct a virtual system, we use a virtual map Φ_R based on the transformations in Example 5: for any $p \in P$, we choose the transformations γ_p and ρ_p to be γ_{ct} and ρ_{ct} of Example 5 with p^* being p . The resulting

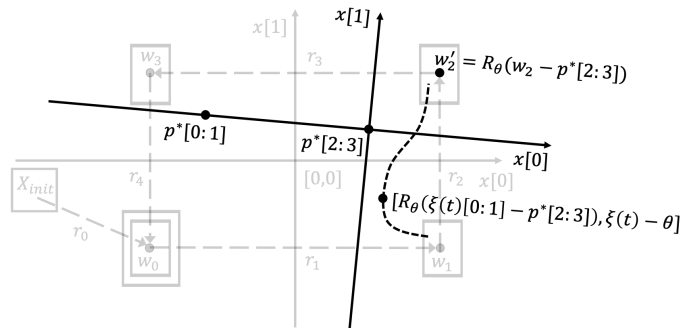


Fig. 5: Changing the axes of the coordinate system so that: the segment connecting $p^*.src = p^*[0:1]$ to $p^*.dest = p^*[2:3]$ is the new $x[0]$ -axis and $p^*.dest$ is the new origin. Such a transformation does not affect the intrinsic behavior of the robot, but only transforms the states in its trajectories to conform with the new coordinate system. Such a coordinate transformation is a valid symmetry.

virtual automaton would be: $R_v = \langle X_v, P_v, X_{init,v}, p_{init,v}, E_v, guard_v, reset_v, f_v \rangle$, where

- (a) $X_v = X = \mathbb{R}^3$ and $P_v = \{p_{v,0} = [-\sqrt{5}, 0, 0, 0], p_{v,1} = [-3, 0, 0, 0], p_{v,2} = [-5, 0, 0, 0]\}$,
- (b) $X_{init,v} = \gamma_{p_{init}}(X_{init})$ and $p_{init,v} = rv(p_{init}) = p_{v,0}$,
- (c) $E_v = \{e_{v,0} = [p_{v,0}, p_{v,1}], e_{v,1} = [p_{v,1}, p_{v,2}], e_{v,2} = [p_{v,2}, p_{v,1}]\}$,
- (d)

$$guard_v(e_{v,i}) = \begin{cases} \mathbf{R}_{\arctan_2(-1,2)}B(p_{v,i}.dest, \varepsilon_0) \times \mathbb{R}, & \text{if } i = 0, \\ \mathbf{R}_0B(p_{v,i}.dest, \varepsilon_1) \times \mathbb{R}, & \text{if } i = 1, \\ \mathbf{R}_{\pi/2}B(p_{v,i}.dest, \varepsilon_1) \times \mathbb{R}, & \text{if } i = 2, \end{cases}$$

where $p_{v,i} = e_{v,i}.src, \forall i \in [3]$,

- (e) $\forall x_v \in X_v$,

$$reset_v(x_v, e_{v,i}) = \begin{cases} \{\gamma_{p_1}(\gamma_{p_0}^{-1}(x_v))\}, & \text{if } i = 0, \\ \{\gamma_{p_2}(\gamma_{p_1}^{-1}(x_v)), \gamma_{p_4}(\gamma_{p_3}^{-1}(x_v))\}, & \text{if } i = 1, \\ \{\gamma_{p_3}(\gamma_{p_2}^{-1}(x_v)), \gamma_{p_4}(\gamma_{p_1}^{-1}(x_v))\}, & \text{if } i = 2, \end{cases}$$

- (f) $\forall x_v \in X_v, \forall p_v \in P_v, f_v(x_v, p_v) = f(x_v, p_v.dest)$.

The resets of the guards of the three edges in E_v constitute the set of all possible reseted states. They are shown as the rectangles on the $x[0]$ -axis, but not at the origin, in Figure 6b.

The new virtual automaton R_v has three modes and three edges versus the single mode and single edge of W_v . However, R_v has guards and reseted guards of smaller volume. To see that, check Figure 3b and compare it with Figure 6b. In Figure 3b, the reset of the guard of the only edge consists of four rectangles, from which the trajectory of the mode p_v can start. That in addition to the initial set X_{init} . On the other hand, in Figure 6b, R_v has three modes and three edges. Yet, the guards and reseted guards are overlapping. This suggests that the reach set of R_v has a smaller volume than that of W_v . That in turn means that the reach set computation would be generally easier and faster for R_v than that for W_v , W , and R .

VI. FASTER SAFETY VERIFICATION USING SYMMETRY-BASED ABSTRACTION

In this section, we show an example application of the abstraction in accelerating safety verification of hybrid automata.

The key factors that motivate this section are: (a) in general, the computation of the reachset of the virtual automaton \mathcal{A}_v reaches a fixed point faster than that of the concrete one \mathcal{A} , (b) one can obtain the reachset of the concrete automaton $\text{Reach}_{\mathcal{A}}$ by transforming the reachset of the virtual one $\text{Reach}_{\mathcal{A}_v}$, and (c) in general, transforming reachsets is computationally cheaper than computing them from scratch.

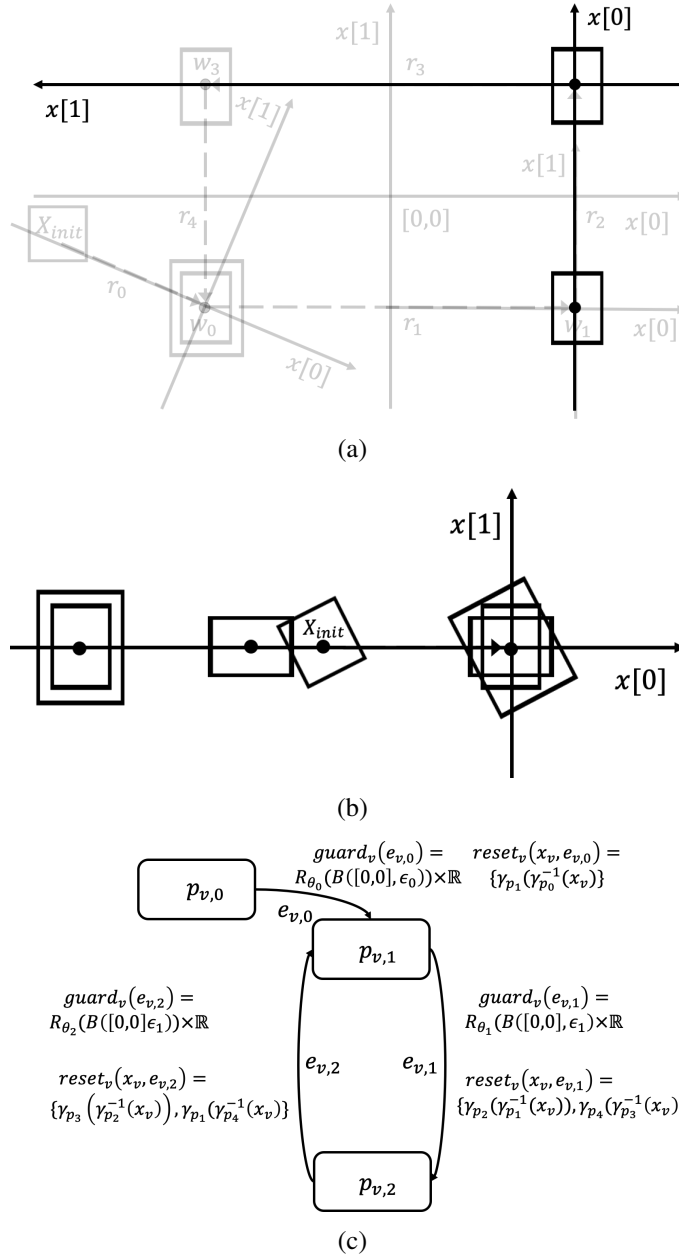


Fig. 6: (6a) the symmetry transformation that changes the coordinate system of the plane of Figure 1a so that r_2 is the new $x[0]$ -axis and waypoint w_2 is the new origin. (6b) shows the virtual initial set, guards and reseted guards of the virtual automaton of Figure 1a after choosing the virtual map to be the set of coordinate transformations to the roads. (6c) shows the resulting hybrid automaton R_v , where $\theta_0 = \arctan_2(r_0.dest[1] - r_0.src[1], r_0.dest[0] - r_0.src[0])$, $\theta_1 = \arctan_2(r_1.dest[1] - r_1.src[1], r_1.dest[0] - r_1.src[0])$, $\theta_2 = \arctan_2(r_2.dest[1] - r_2.src[1], r_2.dest[0] - r_2.src[0])$.

Before delving into the details, in this section, we add the assumption that the modes of \mathcal{A} have time bounds $tbound : P \rightarrow \mathbb{R}^+$. Thus, guards may be ignored only up to a point¹. However, once the total time in mode p reaches $tbound(p)$, the trajectory must stop. If the time bound is reached and some of the guards are satisfied, then \mathcal{A} transitions over any of the corresponding edges nondeterministically. Otherwise, the execution stops. Accordingly, we adjust the definition of \mathcal{A}_v in Definition 5 to include time bounds $tbound_v : P_v \rightarrow \mathbb{R}^+$ on the virtual modes. Specifically, for any $p \in P_v$,

$$tbound_v(p_v) = \max_{p \in rv^{-1}(p_v)} tbound(p). \quad (16)$$

¹This is a simplification for analysis but would not hurt generalizability as the same mode can be visited several times. The results of the paper extend naturally to models with urgent transitions.

It is easy to see that the FSR in Theorem 3 is still valid.

A. Safety verification problem: definition, existing solutions, and their challenges

The *bounded safety verification* problem is to check if any state reachable by \mathcal{A} within fixed number of transitions is unsafe. That is, given maximum number of transitions J and an unsafe set $U \subseteq X$, the problem is to check whether: $\text{Reach}_{\mathcal{A}}(J) \cap U = \emptyset$. In the *unbounded* version of the problem, the number of transitions may be infinite, and we replace the bounded reachset with the unbounded one $\text{Reach}_{\mathcal{A}}$.

For any path $pseq = \{p_i\}_{i \in [J]}$, existing reachability analysis tools compute the reachsets of the modes sequentially. Roughly, for each index $i \in [J]$ in the path, they compute the reachset, or an over-approximation, of the i^{th} mode reachset $\text{Reach}_{\mathcal{A}, pseq, i}$, intersect $\text{Reach}_{\mathcal{A}, pseq, i}$ with $\text{guard}(pseq[i], pseq[i+1])$, and then apply *reset* to the result of the intersection to get the initial set of states for the next mode $pseq[i+1]$ in the path. Consequently, the reachset of the path would be:

$$\text{Reach}_{\mathcal{A}, pseq} = \bigcup_{i \in [J]} \text{Reach}_{\mathcal{A}, pseq, i}. \quad (17)$$

We call the modes reachsets $\text{Reach}_{\mathcal{A}, pseq, i}$ *reachset segments*. Moreover, the reachset of the hybrid automaton $\text{Reach}_{\mathcal{A}}$ would be:

$$\text{Reach}_{\mathcal{A}}(J) = \bigcup_{pseq \in \text{Paths}_{\mathcal{A}}(J)} \text{Reach}_{\mathcal{A}, pseq}, \quad (18)$$

where $\text{Paths}_{\mathcal{A}}(J)$ is the set of all paths of length J of \mathcal{A} .

As J grows, sequential computation of the per-mode reachsets becomes infeasible. Some existing theorems for unbounded reachset computation, such as Theorem 4.4 in [50], assume that the unbounded-time reachset is a bounded set, so that a fixed point can be checked. However, the reachset $\text{Reach}_{\mathcal{A}}$ may become unbounded, which motivates the search for new approaches for unbounded safety verification. That is what we tackle in this section.

B. Relation between concrete and virtual automata reachset segments

The ability of symmetry maps to transform solutions to other solutions of the system extends to transforming reachsets to other reachsets of the system. The following theorem, restated from [42], formalizes this for parameterized dynamical systems.

Theorem 5 (Theorem 2 in [42]) If (1) is Γ -equivariant, then for any $\gamma \in \Gamma$ and its corresponding ρ , any initial set $K \subseteq X$, mode $p \in P$, and $T \geq 0$,

$$\text{Reach}(\gamma(K), \rho(p), T) = \gamma(\text{Reach}(K, p, T)),$$

where $\text{Reach}(K, p, T)$ is the reachset of (1) starting from K , having mode p , and a time bound T .

C. Relation between concrete and virtual automata reachsets

Consider any algorithm or tool that computes the reachset of a hybrid automaton as in equations (17) and (18). Lets call it `computeReachset` and call its output *globalR*. We use `computeReachset` to compute the reachset of the virtual automaton \mathcal{A}_v . We annotate `computeReachset` to keep track of the union of the initial sets and the union of the reachsets being computed corresponding to each unique mode $p_v \in P_v$, in a data structure and call it *Dictionary*. For every $p_v \in P_v$, it stores the initial set in the first argument, which we denote by $\text{Dictionary}[p_v].K$, and the reachset in the second argument, which we denote by $\text{Dictionary}[p_v].R$. After each computation of a new reachset, or an over-approximation thereof, $\text{Reach}_{\mathcal{A}_v, pseq_v, i}$ of a mode in a path, it gets added to the entry corresponding to $pseq_v[i]$ in *Dictionary*. Then, *Dictionary* is used to check if a fixed point of the automaton reachset *globalR*, has been reached. This checks if continuing running of `computeReachset` would not change *globalR*, and then stopping the run accordingly.

Our check for the fixed point is implemented in the function *checkFixedPoint*. It takes as input *Dictionary* and a hybrid automaton for which we are computing the reachset, here \mathcal{A}_v , and returns True or False.

The function $checkFixedPoint(Dictionary)$ returns True if and only if: $X_{init,v} \subseteq Dictionary[p_{init,v}].K$ and $\forall p_v \in P_v$,

$$\begin{aligned} & \cup_{p'_v \in inModes(p_v)} reset(Dictionary[p'_v].R \cap guard(p'_v, p_v), (p'_v, p_v)) \\ & \subseteq Dictionary[p_v].K, \end{aligned} \quad (19)$$

where $inModes(p_v) = \{p'_v \in P_v \mid (p'_v, p_v) \in E_v\}$, and returns False, otherwise.

Theorem 6: If $checkFixedPoint(Dictionary)$ returned True, then for all $pseq_v \in Paths_{\mathcal{A}_v}$, and $i \in [pseq_v.len]$,

$$Reach_{\mathcal{A}_v, pseq_v, i} \subseteq Dictionary[pseq_v[i]].R, \text{ and} \quad (20)$$

$Reach_{\mathcal{A}_v} \subseteq globalR$.

Proof: (Sketch) Recall that we assume that computeReachset is a sound algorithm for computing reachsets of any hybrid automaton. Thus, for every $p_v \in P_v$, $Dictionary[p_v].R$ is an over approximation of the reachset of (4) starting from $Dictionary[p_v].K$ and running for time bound $tbound_v[p_v]$. Now, we fix any path $pseq_v \in Paths_{\mathcal{A}_v}$. The proof is by induction over the indices of $pseq_v$.

Base condition: for $i = 0$, $Reach_{\mathcal{A}_v, pseq_v, i} \subseteq Dictionary[i].R$, by the soundness of computeReachset and the assumption that $X_{init,v} \subseteq Dictionary[p_{init,v}].K$ in equation (20).

Hypothesis: fix an index $i \geq 0$. Assume that the theorem is satisfied for all previous indices $i' \leq i$.

Induction: we want to prove that $Reach_{\mathcal{A}_v, pseq_v, i+1} \subseteq Dictionary[pseq_v[i+1]].R$.

We know from equation (17) and the discussion there, that the initial set of the $(i+1)^{th}$ mode in $pseq_v$ is $reset(Reach_{\mathcal{A}_v, pseq_v, i} \cap guard(pseq_v[i], pseq_v[i+1]), (pseq_v[i], pseq_v[i+1]))$. But, we know from the induction assumption that $Reach_{\mathcal{A}_v, pseq_v, i} \subseteq Dictionary[pseq_v[i]].R$. Moreover, we know from equation (19) that $reset(Dictionary[pseq_v[i]].R \cap guard(pseq_v[i], pseq_v[i+1]), (pseq_v[i], pseq_v[i+1])) \subseteq Dictionary[pseq_v[i+1]].K$. Hence, $reset(Reach_{\mathcal{A}_v, pseq_v, i} \cap guard(pseq_v[i], pseq_v[i+1]), (pseq_v[i], pseq_v[i+1])) \subseteq Dictionary[pseq_v[i+1]].K$. Using the soundness of computeReachset again results in $Reach_{\mathcal{A}_v, pseq_v, i+1} \subseteq Dictionary[pseq_v[i+1]].R$. Hence, (20) is satisfied.

Since the path chosen is arbitrary and the automaton reachset is the union of the path reachsets per equation (18), then $Reach_{\mathcal{A}_v} \subseteq globalR$. ■

Corollary 7: Let $Dictionary$ be the result after reaching a fixed point in computing $Reach_{\mathcal{A}_v}$. Then, for any $J \in \mathbb{N}$ and path $pseq \in Paths_{\mathcal{A}}(J)$ of the concrete automaton \mathcal{A} ,

$$Reach_{\mathcal{A}, pseq} \subseteq \cup_{i \in [J]} \gamma_{pseq[i]}^{-1}(Dictionary[pseq_v[i]]), \quad (21)$$

where $pseq_v[i] = rv(pseq[i])$.

Proof: It follows from Theorem 5, Theorem 6, and the invertibility assumption on γ_p , $\forall p \in P$. ■

Hence, we can compute an over-approximation of the reachset of the concrete automaton \mathcal{A} by running computeReachset to compute $Reach_{\mathcal{A}_v}$ and get its $Dictionary$, iterate over all the paths of \mathcal{A} , transform back the corresponding reachset from $Dictionary$ at each mode visited to get the reachset segment. However, we do not need to iterate over them sequentially as they appear in the path, since for any $i \in [J]$, the i^{th} entry of the sequence on the right-hand-side of (21) only depends on $pseq_v[i]$. Therefore, we can get the i^{th} reachset segment of the path by just transforming the corresponding $Dictionary$ entry. The transformation is done using the symmetry in Φ corresponding to the i^{th} mode. Thus, there is no need to compute the whole reachset before reaching the i^{th} mode, to get its reachset. This will be the key result that helps getting unbounded safety results in the next section.

D. Unbounded safety verification of hybrid automata

In this section, we cultivate all the theorems presented to verify the safety of hybrid automata with symmetric continuous dynamics. Our approach is summarized in Algorithm 1, which we name unboundedVerif. We use the symbol \rightsquigarrow to denote that there exists a path from the source mode to the destination one in \mathcal{A} .

Algorithm 1 unboundedVerif

```

1: input:  $\mathcal{A}, \Phi, U, J$ 
2:  $\mathcal{A}_v \leftarrow \text{constructVirtualModel}(\mathcal{A}, \Phi)$ 
3:  $\text{Dictionary}_v \leftarrow \text{computeReachset}(\mathcal{A}_v, J)$ 
4: if not  $\exists p \in P, p_{init} \rightsquigarrow p$ , and  $\gamma_p^{-1}(\text{Dictionary}[rv(p)].R) \cap U \neq \emptyset$ , then
5:   return: safe
6: else return: unknown

```

The following theorem shows the soundness of unboundedVerif. It follows from Theorem 6 and Corollary 7.

Theorem 8 (main theorem) Given any hybrid automaton \mathcal{A} , virtual map Φ , an unsafe set $U \subseteq X$, and a $J \in \mathbb{N} \cup \{\infty\}$, if unboundedVerif returned *safe*, then $\text{Reach}_{\mathcal{A}}(J) \cap U = \emptyset$.

There is still a possibility that computeReachset would not reach a fixed point in the case of infinite J , in that case, the result is also unknown as well. In that case, the computed reachset should be refined to reduce its over-approximation error, for example, by partitioning the initial set [37], [50] or having higher order Taylor series approximations [51]. Or, the abstraction should be refined, for example, by utilizing more symmetry properties.

The significance of the theorem is that, once a fixed point in computing $\text{Reach}_{\mathcal{A}_v}$ is reached and resulted in *Dictionary*, the safety verification problem gets reduced from computing a sequence of reachset segments and intersections with the guards, to searching over the modes if their transformations of their corresponding segments in *Dictionary* would intersect the unsafe set. For example, assume that the fixed point has been reached after computing five reachset segments. We would be able to compute the reachset segment, or an over-approximation of it, of the hundredth mode in the path of the concrete system, without computing the ninety nine segments of the modes visited before reaching it, but only by transforming one of the five stored segments. For infinite J , one can use a Satisfiability Modulo Theory (SMT) solver, for example, to search for a symmetry map γ_p in Φ corresponding to a mode p in an infinite path of \mathcal{A} , that makes $\gamma_p^{-1}(\text{Dictionary}[rv(p)].R) \cap U \neq \emptyset$.

VII. EXPERIMENTAL EVALUATION

We implemented unboundedVerif in Section VI-D in Python 3, for finite J . Our implementation includes: (1) the function constructVirtualModel, that constructs the virtual automaton \mathcal{A}_v from a given concrete automaton \mathcal{A} and virtual map Φ , (2) the function computeReachset(\mathcal{A}_v, J), which computes the reachset of \mathcal{A}_v using CacheReach [42] for finite J transitions while checking for fixed point as in equation (19), and (3) the data structure *Dictionary* which caches computed reachset segments as in Section VI-D.

We ran several experiments to illustrate the usability and advantage of our method over existing ones. Moreover, we illustrate the key parameters that affect the effectiveness of our abstraction and the quality of our results.

A. Implementation details

The inputs of our implementation are a *scenario* and *dynamics* files describing the hybrid automaton \mathcal{A} and the virtual map Φ . Its outputs are the virtual automaton \mathcal{A}_v and its reachset segments stored in *Dictionary*, the reachset of \mathcal{A} , and the safety decision.

The scenario file specifies \mathcal{A} that is: initial set X_{init} as a hyper-rectangle, unsafe set U as a list of hyperrectangles, set of modes P as a list of tuples, path as a finite sequence of modes $path = \{p_i\}_{i=0}^{J-1}$, guards as a list of hyper-rectangles, and time bounds *tbound* as a list of floats.

The dynamics file specifies the dynamic function f , which given a state x and mode p , returns $f(x, p)$. It has also three other functions that implement the virtual map Φ . The first two functions, given a mode

$p \in P$ and a set of states S that is represented as a Tulip polytope² [52], one returns $\gamma_p(S)$ and the other $\gamma_p^{-1}(S)$. The third function, given a mode $p \in P$, would return $rv(p) = \rho_p(p)$.

Our implementation has 3 options for computing $\text{Reach}_{\mathcal{A}}$:

- the standard method without symmetry (NOSYM or NS),
- the method of [42] using symmetry and caching (SYMCACHE or SC), and
- unboundedVerif (Algorithm 1, SYMVIR or SV).

Reachability analysis: To fix the over-approximation error added by the reachability analysis tool used, our implementation grids both the state space X of \mathcal{A} and the state space X_v of \mathcal{A}_v into equally-sized cells. Then, for NS, while computing $\text{Reach}_{\mathcal{A}}$ as in Section VI-A, for any initial set K for which a reachset segment has to be computed, it checks which cells of the grid over X are occupied by K . For SC, it would transform K using Φ to get the initial set K_v in X_v . After that, it check which cells of the grid over X_v are occupied by K_v . For SV, while computing $\text{Reach}_{\mathcal{A}_v}$, for any initial set K_v in X_v for which a reachset segment has to be computed, it checks which cells of the grid over X_v are occupied by K_v . Then, for NS, it computes the reachsets for each of these cells, and unions the results. For SC and SV, it checks first which cells have their reachsets computed before and cached. For those cells, the reachsets are retrieved from the cache instead of computed. For cells with no cached reachsets, they get computed and cached. After that, our implementation unions the cells reachsets and transform the result back to X using Φ . Doing this would fix the over-approximation error added by the reachability analysis tool, since that depends on the size of the initial set it is asked to compute the reachset for. Thus, fixing the grid size would enable quantifying the over-approximation error added because of using symmetry after fixing the error added by the reachability tool. Moreover, this would allow for a fairer comparison of computation time between the methods.

For SV, after reaching a fixed point in the computation of $\text{Reach}_{\mathcal{A}_v}$, the resulting *Dictionary* is used to get the reachset segments of \mathcal{A} , without the griding-based method described.

Any of the existing reachability analysis tools can be used, such as DryVR [30] and Flow* [51]. Our implementation has both of these tools as options for the user. However, for comparison purposes in our experiments, it simulates the continuous dynamics from the center state of a given cell using an ODE solver, and then places hyper-rectangles equal to the size of the cell at each state in the simulation. The union of these rectangles is considered the reachset. This is computationally cheaper than any of the existing reachability analysis tools. This will ensure that the computation time improvement of SC and SV over NS is not due to using a computationally expensive reachability tool. Such a tool will make the advantage SC and SV even bigger, as they retrieve and transform some of the reachsets versus computing them.

Finally, to check if a scenario is safe, our implementation intersects the computed reachset and the unsafe set.

B. Scenarios and metrics

We consider several scenarios and virtual maps in our experiments, with the following features:

- 1) *dynamic* function of the agent in the scenario: (a) *robot*, that of equation (12) of Example 4, and (b) *linear*, the linear stable dynamics of the form $x = \text{diag}([-3, -3, -1])(x - p)$, where x and $p \in \mathbb{R}^3$,
- 2) *path* followed by the agent as a sequence of modes: (a) *rectangle* (rect.), that of Figure 1a followed for 4 full turns for a total of 16 roads, (b) *Koch snowflake* (Ko.), a truncated Koch snowflake³ path with 16 roads (see Figure 7g), (c) *random* (rand.), a random path of 14 roads (see Figure 7c), and (d) finally, *S-shaped*, an S-shaped path with 16 roads (see Figure 7k),
- 3) virtual map Φ used to construct \mathcal{A}_v : (a) *T*, translation map that translates the coordinates of both waypoints of a road so that the end point is the origin, and (b) *TR*, combines *T* with rotation of axes

²<https://tulip-control.github.io/polytope/>

³The actual Koch snowflake is a fractal. Here we truncate the construction after a finite number of iterations to get a snowflake shape with finite edges.

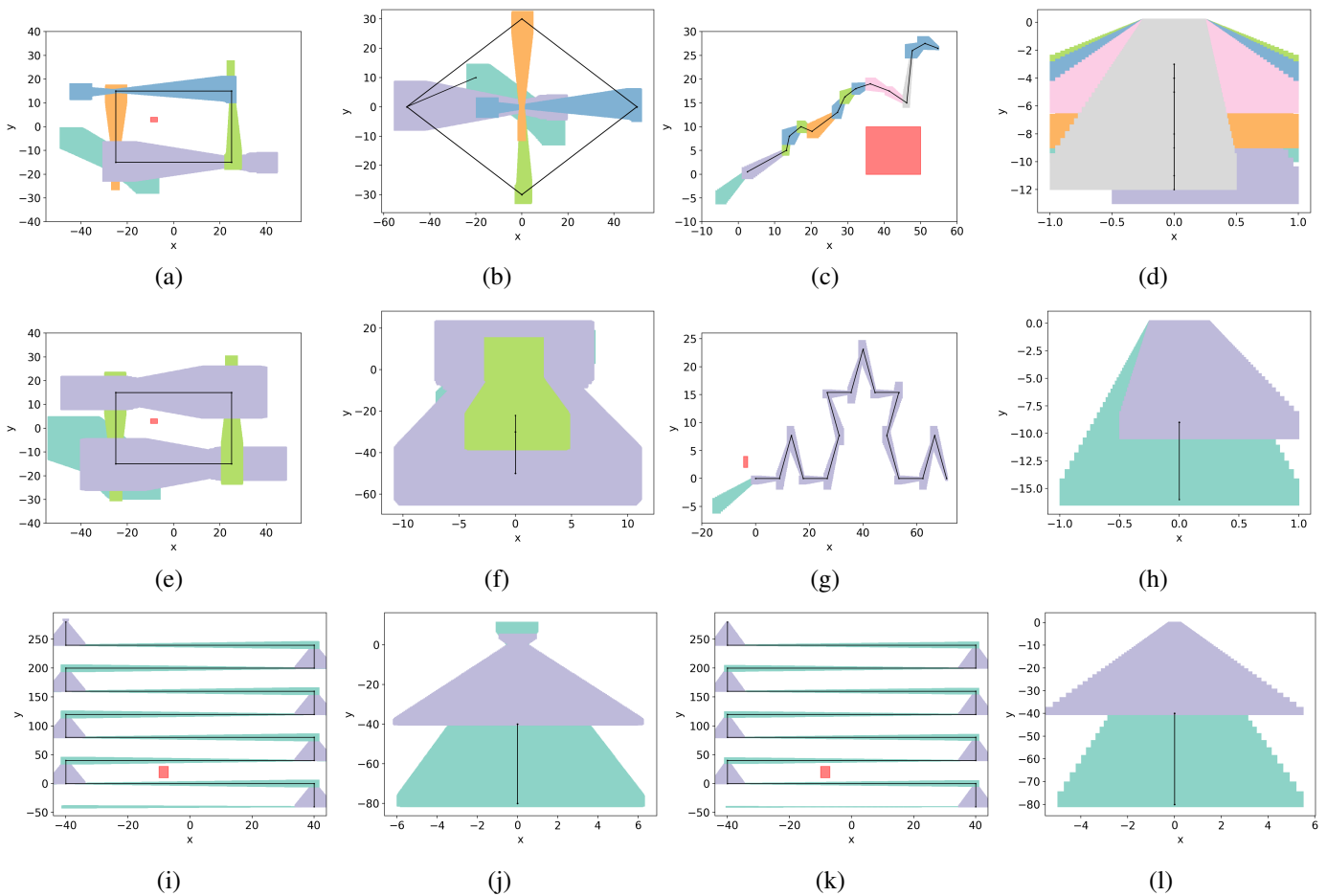


Fig. 7: Reachsets, projected to the position-in-the-plane part of the state, for vehicles visiting sequences of waypoints. Each horizontal pair depicts $\text{Reach}_{\mathcal{A}}$ (left) and $\text{Reach}_{\mathcal{S}_v}$ (right) of a scenario. sym is SV in all scenarios. dynamic is *robot* (left) and *linear* (right). Φ is T in the 1st row (Figures 7a through 7d), and TR in the rest of the figures (Figures 7e through 7l). Figure 7b has larger $\#m/e$ and smaller reachset segments than Figure 7f, while modeling the same scenario, where path is *rectangle*, as shown in Figures 7a and 7e. That shows that smaller $\#m/e$ means larger reachset segments. Figure 7d, corresponding to path being *random* in Figure 7c, has larger $\#m/e$ than 7h, corresponding to path being *snowflake* in Figure 7g, respectively. That shows that when Φ can relate the trajectories of more modes, it results in smaller $\#m/e$. Figure 7j with dynamic being *robot* has larger reachset segments than 7l with dynamic being *linear*, while corresponding to the same S-shaped path. That shows that more complex dynamics results in larger reachset segments.

so that the road is the new $x[1]$ -axis. That is in contrast with Example 5, where we chose the road to be the $x[0]$ -axis, and

4) $\text{sym} \in \{\text{NS}, \text{SC}, \text{SV}\}$, method used to compute $\text{Reach}_{\mathcal{A}}$.

For each of the scenarios, we collected several statistics:

- 1) *computed* ($\#co$), *retrieved* ($\#re$), *copied* ($\#cp$), *total* ($\#tot$): are the numbers of cells reachsets that has been computed from scratch, has been retrieved from the cache, number of reachset segments that has been transformed from *Dictionary*, after a fixed point has been reached, and the sum of all three numbers, respectively,
- 2) $\#m/e$, are the numbers of modes and edges of \mathcal{A}_v ,
- 3) *time*, in minutes, is the total time needed to compute the reachset of \mathcal{A} , and
- 4) *over-approximation error* (%) is the error added to the reachset of \mathcal{A} , due to using symmetry:

$$\text{error} = \text{avg}_{i \in [\text{path.len}]} \frac{\text{Vol}(K_{j,i}) - \text{Vol}(K_{\text{NS},i})}{\text{Vol}(K_{\text{NS},i})} \times 100,$$

where $\text{Vol}(\cdot)$ returns the volume of the given hyperrectangle and $K_{j,i}$ denotes the i^{th} mode initial set of the path using method $j \in \{\text{NS}, \text{SC}, \text{SV}\}$.

C. Results analysis and discussion

We will discuss several observations using the results of some experiments. To check the same observations for different scenarios, we refer the reader to Table V in the Appendix.

SV vs. NS and SC: The results of running our implementation on a scenario using all combinations of the three methods with the two virtual maps, are shown in Table I. When using the SV, the numbers of computed reachsets $\#co$ are 1749 and 1513, for Φ being T and TR , respectively. These are significantly smaller than those when using the other methods in the first three rows. The reason is that 11 out of the 16 segments were transformed from *Dictionary*, when Φ was T , and 13 out of 16 when Φ was TR . Hence, only five segments needed to be computed using the griding method, before a fixed point was reached when Φ was T , and three when Φ was TR . This resulted in significant decrease in the total number of reachsets requested ($\#tot.$). Consequently, the computation time is around 89% and 56% less than that of NS and SC, respectively, when Φ was T , and by 89% and 83%, when Φ was TR . We can see that SC, that uses symmetry and caching, maintained advantage in computation time over NS, the standard one, as in [42].

When using SV, the over-approximation errors were 23% and 140.8%, for Φ being T and TR , respectively. These are larger than those of SC, which were 0% and 49.4%, respectively. This is because of the conservativeness of the abstraction as we discussed at the end of Section IV-B.

TABLE I: Results showing the advantage of using SV over NS and SC to compute $\text{Reach}_{\mathcal{A}_v}$ for the scenario where *dynamic* and *path* are *robot* and *S-shaped*, respectively. $\#m/e$ is $3/4$ and $2/2$ for the 4th and 5th rows, respectively.

Φ	sym	$\#co$	$\#re$	$\#cp$	$\#tot.$	time	error
-	NS	18591	-	-	18591	1.3	-
T	SC	6831	11760	-	18591	0.8	0
TR	SC	2421	3864	-	6285	0.32	49.3
T	SV	1749	84	11	1844	0.14	23.4
TR	SV	1513	0	13	1526	0.14	140.8

Smaller vs. larger virtual automata: In general, the fewer the modes and edges $\#m/e$ of \mathcal{A}_v , the less is the number of reachset segments have to be computed before reaching a fixed point. This can be seen, for example, by comparing the 4th and 5th rows of Table I. In the 4th row, where Φ was T , $\#m/e$ were $3/4$. In the 5th row, where Φ was TR , $\#m/e$ were $2/2$. Out of the 16 reachset segments had to be computed for the 16 roads in the *S-shaped* path, in the 4th row, 11 segments were transformed from *Dictionary*, while in the 5th row, 13 segments. That means that the fixed point was reached earlier when $\#m/e$ of \mathcal{A}_v were smaller.

On the other hand, smaller $\#m/e$ means larger equivalent sets of modes and edges in \mathcal{A} . Hence, more modes of \mathcal{A} would be mapped to the same mode of \mathcal{A}_v . That means each reachset segment in *Dictionary* should cover more cases. That leads to larger reachset segments and more conservativeness of the abstraction. This can be seen by comparing the over-approximation error in the 4th and 5th rows. In the 5th row, it had 140.8% error versus 23.4% of the 4th row. It can also be seen for the rectangle path with robot dynamics scenario by checking Figures 7a and 7e. Figure 7e has smaller $\#m/e$, but larger reachset than Figures 7a.

Additionally, the larger $\#m/e$, the more expensive the fixed point check of equation (19) is. This can be seen by again comparing the 4th and 5th rows. The 4th row had larger $\#co$ and $\#tot.$ than the 5th row, and the latter reached fixed point earlier. Both of these reasons should have lead the 5th row to have faster computation time if there was no fixed-point check after each segment computation. However, they were the same.

Larger reachsets are also more expensive to compute since, as mentioned earlier, they are computed as a union of reachsets with smaller initial sets of fixed size, the grid cells size. Thus, more cells reachsets are computed because of larger reachsets causing larger per-mode initial sets. This overhead would lead to larger computation time for some of the scenarios with smaller \mathcal{A}_v than those with larger ones, despite

reaching the fixed point earlier. For example, the computation time for the 3rd row was larger than that of the 2nd row in Table II, although the former had smaller \mathcal{A}_v and reached fixed point earlier.

TABLE II: Results showing that smaller $\#m/e$ might cause more computations and larger reachsets than one with larger $\#m/e$. Scenario has *dynamic* and *path* being *robot* and *rectangle*, respectively. NS is used in the 1st row and SV in the 2nd and 3rd rows.

Φ	$\#m/e$	#co	#re	#cp	#tot.	time	error
-	-	8001	-	-	8001	0.6	-
T	5/5	9306	0	11	9317	0.84	326
TR	3/3	30456	273	13	30742	3.42	2142

Effective vs. less effective symmetries: The more effective Φ is in grouping different modes of \mathcal{A} , the smaller \mathcal{A}_v is. In other words, the coarser the partition of P that Φ creates, the smaller are $\#m/e$. This can be seen in our experiments by comparing $\#m/e$ for Φ being T or TR for the scenarios in Tables I and II. For example, in Table II, $\#m/e = 5/5$ when Φ is T , and $\#m/e = 3/3$, when Φ being TR . This reflects that TR is able to group more modes than T . This is expected since TR relates translated and rotated trajectories of the robot, not just translated ones. Another point of view can be seen by examining the scenarios considered in Table III. Although the total number of segments for the Koch-snowflake path is 16, larger than that of the random path which is 14, $\#m/e$ of the latter were 7/11, much larger than those of the former 2/2. This can also be seen by comparing Figures 7h and 7d. That means that TR was not able to group the different modes of the random path, due to the different lengths of the roads. On the other hand, it was able to group all the modes of the snowflake path in two modes, since all the roads, except the first, are translated and rotated versions of each other.

TABLE III: Results showing that $\Phi = TR$ results in smaller \mathcal{A}_v , i.e. smaller $\#m/e$, than $\Phi = T$. Dynamics are linear and *sym* is SV.

path	Φ	$\#m/e$	#co	#re	#cp	#tot.	time
rand.	T	12/13	321	93	0	414	0.29
rand.	TR	7/11	228.6	224.4	2	455	0.33
Ko.	T	6/8	392	208	4	604	0.39
Ko.	TR	2/2	180	0	2	194	0.17

Simple vs. complex continuous dynamics: The more complex the continuous dynamics are, the more the cells reachsets have to be computed. This is shown by comparing $\#tot.$ of the linear and robot dynamics in Table IV. They have the same sizes of initial sets, same $\#m/e$, and they reach the fixed point after the same number of reachset segments. Yet, the robot had $\#tot.$ of 1844 versus 654 for the linear dynamics. Also, this can be seen by comparing the sizes of the reachsets of Figures 7j and 7l. The green reachset segment of the robot has an initial set width from -6 to 6, while that of the linear model ranges from around -5 to 5. That is because the robot is less stable than the linear one.

TABLE IV: Results showing that stable linear dynamics results in fewer reachsets need to be computed, than the more complex robot dynamics. *path* is *S-shaped*.

dyn.	Φ	# co	# re	# cp	# tot.	time	error
robot	T	1749	84	11	1844	0.14	23.4
robot	TR	1513	0	13	1526	0.14	140.8
linear	T	603	40	11	654	0.46	7.3
linear	TR	601	36	13	650	0.45	103.8

VIII. CONCLUSION

We presented the first symmetry-based abstractions of hybrid automata. Our abstractions create automata with fewer number of modes and edges than the concrete ones by representing sets of modes with

single ones. Symmetry maps transform trajectories of a concrete mode to trajectories of its corresponding abstract one, and vice versa. We showed a forward simulation relation that proves the soundness of our abstraction. Moreover, we showed how these abstractions would accelerate reachset computation and enable unbounded-time safety verification. The fewer number of modes of the abstract automaton makes its reachset computation reach a fixed point earlier than that of the concrete one. Such a fixed point would result on a per-mode reachsets that can be transformed to construct the reachset of any concrete mode. We implemented our approach in Python 3 and showed the advantage of our approach over existing methods and the different parameters that affect our abstraction quality, in a sequence of reachability analysis experiments.

REFERENCES

- [1] R. Goebel, R. G. Sanfelice, and A. R. Teel, *Hybrid Dynamical Systems: Modeling, Stability, and Robustness*. Princeton University Press, 2012. [Online]. Available: <http://www.jstor.org/stable/j.ctt7s02z>
- [2] A. van der Schaft and H. Schumacher, *An Introduction to Hybrid Dynamical Systems*. London: Springer, 2000.
- [3] R. Alur, *Principles of Cyber-Physical Systems*. The MIT Press, 2015.
- [4] T. A. Henzinger, P. W. Kopke, A. Puri, and P. Varaiya, “What’s decidable about hybrid automata?” *Journal of Computer and System Sciences*, vol. 57, pp. 94–124, 1998.
- [5] R. Alur, T. Henzinger, G. Lafferriere, and G. Pappas, “Discrete abstractions of hybrid systems,” in *Proceedings of the IEEE*, 2000.
- [6] R. Alur, C. Courcoubetis, N. Halbwachs, T. A. Henzinger, P.-H. Ho, X. Nicollin, A. Olivero, J. Sifakis, and S. Yovine, “The algorithmic analysis of hybrid systems,” *Theoretical Computer Science*, vol. 138, no. 1, pp. 3–34, 1995.
- [7] V. Vladimerou, P. Prabhakar, M. Viswanathan, and G. E. Dullerud, “STORMED hybrid systems,” in *Automata, Languages and Programming, ICALP 2008*, ser. LNCS, vol. 5126. Springer, 2008, pp. 136–147.
- [8] G. Lafferriere, G. J. Pappas, and S. Sastry, “O-minimal hybrid systems,” *Mathematics of control, signals and systems*, vol. 13, no. 1, pp. 1–21, 2000.
- [9] A. Girard, “Controller synthesis for safety and reachability via approximate bisimulation,” *Automatica*, vol. 48, no. 5, pp. 947 – 953, 2012. [Online]. Available: <http://www.sciencedirect.com/science/article/pii/S000510981200088X>
- [10] P. Tabuada, G. J. Pappas, and P. U. Lima, “Composing abstractions of hybrid systems.” in *HSCC 2002*, ser. LNCS, C. Tomlin and M. R. Greenstreet, Eds., vol. 2289. Springer, 2002, pp. 436–450.
- [11] P. Tabuada and G. J. Pappas, “Hybrid abstractions that preserve timed languages,” in *Proceedings of the 4th International Workshop on Hybrid Systems: Computation and Control*, ser. HSCC ’01. Berlin, Heidelberg: Springer-Verlag, 2001, p. 501–514.
- [12] A. Fehnker, E. M. Clarke, S. K. Jha, and B. H. Krogh, “Refining abstractions of hybrid systems using counterexample fragments,” in *HSCC’2005*, ser. Lecture Notes in Computer Science, M. Morari and L. Thiele, Eds., vol. 3414. Springer, 2005, pp. 242–257.
- [13] R. Alur, T. Dang, and F. Ivančić, “Counterexample-guided predicate abstraction of hybrid systems,” *Theoretical Computer Science*, vol. 354, no. 2, pp. 250–271, 2006.
- [14] N. Roohi, P. Prabhakar, and M. Viswanathan, “HARE: A hybrid abstraction refinement engine for verifying non-linear hybrid automata,” in *Tools and Algorithms for the Construction and Analysis of Systems - 23rd International Conference, TACAS 2017, Held as Part of the European Joint Conferences on Theory and Practice of Software, ETAPS 2017, Uppsala, Sweden, April 22-29, 2017, Proceedings, Part I*, 2017, pp. 573–588. [Online]. Available: https://doi.org/10.1007/978-3-662-54577-5_33
- [15] P. Prabhakar, P. S. Duggirala, S. Mitra, and M. Viswanathan, “Hybrid automata-based CEGAR for rectangular hybrid systems,” *Formal Methods in System Design*, vol. 46, no. 2, pp. 105–134, 2015. [Online]. Available: <https://doi.org/10.1007/s10703-015-0225-4>
- [16] S. Sankaranarayanan, “Change-of-bases abstractions for non-linear hybrid systems,” *Nonlinear Analysis: Hybrid Systems*, vol. 19, pp. 107 – 133, 2016. [Online]. Available: <http://www.sciencedirect.com/science/article/pii/S1751570X15000540>
- [17] K. Hsu, R. Majumdar, K. Mallik, and A.-K. Schmuck, “Lazy abstraction-based control for safety specifications,” in *57th IEEE Conference on Decision and Control, CDC 2018, Miami, FL, USA, December 17-19, 2018*, 2018, pp. 4902–4907. [Online]. Available: <https://doi.org/10.1109/CDC.2018.8619659>
- [18] T. Dang, O. Maler, and R. Testylier, “Accurate hybridization of nonlinear systems,” 01 2010, pp. 11–20.
- [19] P. Mehta, G. Hagen, and A. Banaszuk, “Symmetry and symmetry-breaking for a wave equation with feedback,” *SIAM J. Applied Dynamical Systems*, vol. 6, pp. 549–575, 01 2007.
- [20] S. Bonnabel, P. Martin, and P. Rouchon, “Symmetry-preserving observers,” *IEEE Transactions on Automatic Control*, vol. 53, no. 11, pp. 2514–2526, 2008.
- [21] M. W. Spong and F. Bullo, “Controlled symmetries and passive walking,” *IEEE Transactions on Automatic Control*, vol. 50, no. 7, pp. 1025–1031, July 2005.
- [22] L. G’erard and J.-J. E. Slotine, “Neuronal networks and controlled symmetries, a generic framework,” 2006.
- [23] J. Hanc, S. Tuleja, and M. Hancova, “Symmetries and conservation laws: Consequences of noether’s theorem,” *American Journal of Physics - AMER J PHYS*, vol. 72, pp. 428–435, 04 2004.
- [24] E. Noether, “Invarianten beliebiger differentialausdrücke,” *Nachrichten von der Gesellschaft der Wissenschaften zu Göttingen, Mathematisch-Physikalische Klasse*, vol. 1918, pp. 37–44, 1918. [Online]. Available: <http://eudml.org/doc/59011>
- [25] G. Frehse, C. L. Guernic, A. Donzé, S. Cotton, R. Ray, O. Lebeltel, R. Ripado, A. Girard, T. Dang, and O. Maler, “SpaceX: Scalable verification of hybrid systems,” in *Computer Aided Verification*, ser. Lecture Notes in Computer Science, G. Gopalakrishnan and S. Qadeer, Eds., vol. 6806. Springer, 2011, pp. 379–395.
- [26] S. Bak and P. S. Duggirala, “Hylaa: A tool for computing simulation-equivalent reachability for linear systems,” in *Proceedings of the 20th International Conference on Hybrid Systems: Computation and Control*. ACM, 2017, pp. 173–178.

- [27] S. Bak, H.-D. Tran, and T. T. Johnson, “Numerical verification of affine systems with up to a billion dimensions,” in *Proceedings of the 22nd ACM International Conference on Hybrid Systems: Computation and Control*, ser. HSCC ’19. New York, NY, USA: Association for Computing Machinery, 2019, p. 23–32. [Online]. Available: <https://doi.org/10.1145/3302504.3311792>
- [28] N. Roohi, Y. Wang, M. West, G. Dullerud, and M. Viswanathan, “Statistical verification of Toyota powertrain control verification benchmark,” in *Proceedings of the 20th international conference on Hybrid systems: computation and control*. ACM, 2017.
- [29] X. Jin, J. V. Deshmukh, J. Kapinski, K. Ueda, and K. R. Butts, “Powertrain control verification benchmark,” in *17th International Conference on Hybrid Systems: Computation and Control (part of CPS Week), HSCC’14, Berlin, Germany, April 15-17, 2014*, 2014, pp. 253–262. [Online]. Available: <https://doi.org/10.1145/2562059.2562140>
- [30] C. Fan, B. Qi, and S. Mitra, “Data-driven formal reasoning and their applications in safety analysis of vehicle autonomy features,” *IEEE Design & Test*, vol. 35, no. 3, pp. 31–38, 2018. [Online]. Available: <https://doi.org/10.1109/MDAT.2018.2799804>
- [31] P. S. Duggirala, C. Fan, S. Mitra, and M. Viswanathan, “Meeting a powertrain verification challenge,” in *Computer Aided Verification - 27th International Conference, CAV 2015, San Francisco, CA, USA, July 18-24, 2015, Proceedings, Part I*, 2015, pp. 536–543. [Online]. Available: https://doi.org/10.1007/978-3-319-21690-4_37
- [32] T. Kushner, B. W. Bequette, F. Cameron, G. P. Forlenza, D. M. Maahs, and S. Sankaranarayanan, “Models, devices, properties, and verification of artificial pancreas systems,” in *Automated Reasoning for Systems Biology and Medicine*, 2019, pp. 93–131. [Online]. Available: https://doi.org/10.1007/978-3-030-17297-8_4
- [33] S. Sankaranarayanan, S. A. Kumar, F. Cameron, B. W. Bequette, G. E. Fainekos, and D. M. Maahs, “Model-based falsification of an artificial pancreas control system,” *SIGBED Review*, vol. 14, no. 2, pp. 24–33, 2017. [Online]. Available: <https://doi.org/10.1145/3076125.3076128>
- [34] R. Grosu, G. Batt, F. H. Fenton, J. Glimm, C. Guernic, S. A. Smolka, and E. Bartocci, “From cardiac cells to genetic regulatory networks,” in *Computer Aided Verification*, ser. Lecture Notes in Computer Science, G. Gopalakrishnan and S. Qadeer, Eds. Springer Berlin Heidelberg, 2011, vol. 6806, pp. 396–411.
- [35] X. Chen, E. Ábrahám, and S. Sankaranarayanan, “Flow*: An analyzer for non-linear hybrid systems,” in *Computer Aided Verification*, ser. Lecture Notes in Computer Science, N. Sharygina and H. Veith, Eds. Springer Berlin Heidelberg, 2013, vol. 8044, pp. 258–263.
- [36] M. Althoff, “An introduction to cora 2015,” in *Proc. of the Workshop on Applied Verification for Continuous and Hybrid Systems*, 2015.
- [37] P. S. Duggirala, S. Mitra, M. Viswanathan, and M. Potok, “C2e2: A verification tool for stateflow models,” in *Tools and Algorithms for the Construction and Analysis of Systems*, C. Baier and C. Tinelli, Eds. Berlin, Heidelberg: Springer Berlin Heidelberg, 2015, pp. 68–82.
- [38] C. Fan, J. Kapinski, X. Jin, and S. Mitra, “Locally optimal reach set over-approximation for nonlinear systems,” in *EMSOFT*. ACM, 2016, pp. 6:1–6:10.
- [39] C. Fan and S. Mitra, “Bounded verification with on-the-fly discrepancy computation,” in *ATVA*, ser. Lecture Notes in Computer Science, vol. 9364. Springer, 2015, pp. 446–463.
- [40] X. Chen, “Reachability analysis of non-linear hybrid systems using taylor models,” 2015.
- [41] H. Sibai, N. Mokhlesi, and S. Mitra, “Using symmetry transformations in equivariant dynamical systems for their safety verification,” in *Automated Technology for Verification and Analysis*, 2019, pp. 1–17.
- [42] H. Sibai, N. Mokhlesi, C. Fan, and S. Mitra, “Multi-agent safety verification using symmetry transformations,” in *Tools and Algorithms for the Construction and Analysis of Systems*, A. Biere and D. Parker, Eds. Cham: Springer International Publishing, 2020, pp. 173–190.
- [43] J. Maidens and M. Arcak, “Exploiting symmetry for discrete-time reachability computations,” 2018.
- [44] R. Alur, C. C. T. A. Henzinger, and P. H. Ho., “Hybrid automata: an algorithmic approach to the specification and verification of hybrid systems,” in *Hybrid Systems*, ser. LNCS, R. L. Grossman, A. Nerode, A. P. Ravn, and H. Rischel, Eds., vol. 736. Springer-Verlag, 1993, pp. 209–229.
- [45] D. K. Kaynar, N. Lynch, R. Segala, and F. Vaandrager, *The Theory of Timed I/O Automata*, ser. Synthesis Lectures on Computer Science. Morgan Claypool, November 2005, also available as Technical Report MIT-LCS-TR-917, MIT.
- [46] S. Mitra, “A verification framework for hybrid systems,” Ph.D. dissertation, Massachusetts Institute of Technology, Cambridge, MA 02139, September 2007. [Online]. Available: <http://people.csail.mit.edu/mitras/research/thesis.pdf>
- [47] S. Blazic, “A novel trajectory-tracking control law for wheeled mobile robots,” *Robotics and Autonomous Systems*, vol. 59, no. 11, pp. 1001 – 1007, 2011. [Online]. Available: <http://www.sciencedirect.com/science/article/pii/S0921889011001023>
- [48] G. Russo and J.-J. E. Slotine, “Symmetries, stability, and control in nonlinear systems and networks,” *Physical Review E*, vol. 84, no. 4, p. 041929, 2011.
- [49] A. Girard, A. A. Julius, and G. J. Pappas, “Approximate simulation relations for hybrid systems,” in *IFAC Analysis and Design of Hybrid Systems*, Alghero, Italy, June 2006.
- [50] C. Fan, B. Qi, S. Mitra, and M. Viswanathan, “Data-driven verification and compositional reasoning for automotive systems,” in *Computer Aided Verification*. Springer International Publishing, 2017, pp. 441–461.
- [51] X. Chen, E. Ábrahám, and S. Sankaranarayanan, “Flow*: An analyzer for non-linear hybrid systems,” in *Computer Aided Verification*, ser. Lecture Notes in Computer Science, N. Sharygina and H. Veith, Eds. Springer Berlin Heidelberg, 2013, vol. 8044, pp. 258–263.
- [52] T. Wongpiromsarn, U. Topcu, N. Ozay, H. Xu, and R. M. Murray, “Tulip: A software toolbox for receding horizon temporal logic planning,” in *Proceedings of the 14th International Conference on Hybrid Systems: Computation and Control*, ser. HSCC ’11. New York, NY, USA: Association for Computing Machinery, 2011, p. 313–314. [Online]. Available: <https://doi.org/10.1145/1967701.1967747>

ACKNOWLEDGMENT

The authors are supported by a research grant from The Boeing Company and a research grant from NSF (CPS 1739966). We would like to thank John L. Olson and Arthur S. Younger from The Boeing Company for valuable technical discussions.

TABLE V: Experimental results.

Scenarios					Results							
id	model	path	virtual map	sym	#co	#ret.	#cp	#tot.	#m/e	# pre-f	time	error
1	robot	rectangle	-	NS	8001	-	-	8001	-	-	0.6	-
2	robot	rectangle	trans	SC	3945	4056	-	8001	-	-	0.42	0
3	robot	rectangle	trans.+rot.	SC	4206	2008	-	6214	-	-	0.43	-30
4	robot	rectangle	trans.	SV	9306	0	11	9317	5/5	5/16	0.84	326
5	robot	rectangle	trans.+rot.	SV	30456	273	13	30742	3/3	3/16	3.42	2142
6	linear	snowflake	-	NS	835	-	-	835	-	-	0.52	-
7	linear	snowflake	trans.	SC	475	388	-	863	-	-	0.52	3.7
8	linear	snowflake	trans.+rot.	SC	234	732	-	966	-	-	0.5	93.5
9	linear	snowflake	trans.	SV	392	208	4	604	6/8	12/16	0.39	3.2
10	linear	snowflake	trans.+rot.	SV	180	0	14	194	2/2	2/16	0.17	137.4
11	linear	random	-	NS	351	-	-	351	-	-	0.23	-
12	linear	random	trans.	SC	321	93	-	414	-	-	0.37	19
13	linear	random	trans.+rot.	SC	186.3	260.7	-	447	-	-	0.28	118.7
14	linear	random	trans.	SV	321	93	0	414	12/13	14/14	0.29	19
15	linear	random	trans.+rot.	SV	228.6	224.4	2	455	7/11	12/14	0.33	165.23
16	linear	S-shaped	-	NS	5963	-	-	5963	-	-	3.85	-
17	linear	S-shaped	trans.	SC	2419	3544	-	5963	-	-	3.14	0
18	linear	S-shaped	trans.+rot.	SC	2167	3808	-	5975	-	-	2.97	0.6
19	linear	S-shaped	trans.	SV	603	40	11	654	3/4	5/16	0.46	7.3
20	linear	S-shaped	trans.+rot.	SV	601	36	13	650	2/2	3/16	0.45	103.8
21	robot	S-shaped	-	NS	18591	-	-	18591	-	-	1.3	-
22	robot	S-shaped	trans.	SC	6831	11760	-	18591	-	-	0.8	0
23	robot	S-shaped	trans.+rot.	SC	2421	3864	-	6285	-	-	0.32	49.3
24	robot	S-shaped	trans.	SV	1749	84	11	1844	3/4	5/16	0.14	23.4
25	robot	S-shaped	trans.+rot.	SV	1513	0	13	1526	2/2	3/16	0.14	140.8